Archives of Civil and Mechanical Engineering (2023) 23:230
https://doi.org/10.1007/s43452-023-00774-9

ORIGINAL ARTICLE

Slag/diatomite-based alkali-activated lightweight composites containing waste andesite sand: mechanical, insulating, microstructural and durability properties

Oguzhan Yavuz Bayraktar[1] · Ugur Yakupoglu[1] · Ahmet Benli[2]

Received: 27 April 2023 / Revised: 15 August 2023 / Accepted: 20 August 2023 / Published online: 29 August 2023

Abstract
Waste andesite sand (AS) is produced when cutting andesite stone and doing other stone dressing procedures. Problems with storage and environmental pollution may result from the disposal of AS. These issues might be resolved using AS in the manufacturing of alkali-activated composites. Pozzolanic powders are used extensively in the construction sector to reduce the need for cement, which lowers the price of making concrete and lessens environmental pollution from CO_2 emissions from cement producers. This paper reports the findings of an experimental examination into the impact of diatomite powder and waste andesite sand on the microstructural, durability, and mechanical characteristics of environmental-friendly alkali-activated lightweight composites (AALC). Ground blast furnace slag (GBFS) and diatomite powder (DP) were used as the main solid precursors, silica sand (SS) and waste andesite sand (AS) were used as fillers for the design of AALC mixtures. The alkaline activators adopted in this study were sodium hydroxide and sodium silicate. Physico-mechanical characteristics, transport properties, thermal conductivity, sorptivity, and drying shrinkage of generated AALC mixes were also examined in addition to its performance under freeze–thaw (F–T) cycles and high temperatures. SEM analyses of the AALC were conducted to investigate the microstructure of the produced specimens. Sixteen AALC mixtures were created using GBFS/DP ratios of 100/0, 90/10, 80/20 and 70/30 and AS was used to replace silica sand (SS) in four different rates of 0%, 25%, 50%, and 100%. Prior to ambient curing, the manufactured samples were cured at 80 °C for 24 h to quicken geopolymerization. The findings showed that the mixture with 100% GBFS and 100% AS had a maximum compressive strength of around 60 MPa. When GBFS was replaced with 20% and 30% DP, the compressive strength of AALC specimens was drastically reduced. The AALC mixtures containing 20% and 30% DP showed the lowest thermal conductivity results. The best high-temperature resistance was demonstrated by the mixture D20A50, which comprises 20% DP and 50% AS and experiences a strength loss of 20.7% at 900 °C. The best resistance to freezing and thawing exposure was found in mixtures that contained 10% DP and 50% AS.

Keywords Lightweight alkali-activated composites · Slag · Diatomite powder · Waste andesite aggregate · Freeze–thaw

1 Introduction

Concrete is recognized as a crucial building material due to its accessibility and several advantages over other materials. Yet, as demand for concrete increases, questions have been raised concerning the use of natural resources and Ordinary Portland Cement (OPC), the cement used in concrete that acts as a binding agent and demands high temperatures for manufacture, significantly increases greenhouse gas emissions. The cement sector is responsible for up to 8% of global CO_2 emissions [1–6]. Since CO_2 is believed to contribute significantly to the generation of greenhouse gases that cause climate change, OPC is recognized as a harmful binder material for the environment [1, 6]. One ton of OPC requires 0.6 to 1 ton of CO_2 to be generated. Global demand for OPC is expected to treble by 2050, which could make it more challenging for current CO_2 emission reduction efforts [7, 8]. Alkali-activated materials (AAMs), green

✉ Ahmet Benli
ahbenli@hotmail.com

[1] Civil Engineering Department, Kastamonu University, 37150 Kastamonu, Turkey

[2] Civil Engineering Department, Bingol University, 12100 Bingol, Turkey

hybrid alkaline cements, geopolymer composites, and other such possibilities have all been studied to look at various sustainable, green cementitious materials that are low-emission, low-carbon, and energy-efficient [9–12]. AAMs have emerged as a fascinating new Portland cement alternative. Low heat conductivity, excellent compressive strength, little shrinkage, quick setting, and reduced environmental impact are just a few of its benefits. There has been a lot of research done to determine whether it is feasible to make alkali-activated cements utilizing different industrial byproducts and natural raw materials. Aluminosilicate materials such as fly ash, metakaolin (MK), granulated blast furnace slag (GBFS), silica fume (SF), and calcined natural kaolinite rocks have all been identified as potential candidates for alkali-activated synthesis [13–16]. Natural sand, which is used as an aggregate in conventional concrete and mortar, is also quickly running out due to the huge demand in the building sector [17]. Since AAMs allow for the use of industrial and municipal waste as a precursor, they are more environmentally sustainable than Portland cement-based materials, which avoids significant CO_2 emissions and excessive energy use. Research on AAMs is, therefore, getting more interest [18, 19].

Natural pozzolanic materials, such as GBFS, silica fume, metakaolin, fly ash, and natural pozzolans (diatomite zeolite, and volcanic tuff), are successfully used as precursors for the creation of AAMs or geopolymers [10, 11, 20–22]. However, there has not been much research on diatomite, a naturally occurring pozzolans that contain highly reactive silica, in geopolymer or AAMs systems. The siliceous skeletal remains of the single-celled creatures known as diatoms make up the natural pozzolans known as diatomite. Numerous minerals, including silica, alumina, and iron oxide, are present in diatomite's structure. Numerous benefits exist for it, including a porous structure, inexpensive price, and high silica content. The production of ceramics, thermal isolation, and the removal of heavy metal ions are further uses for it [23, 24]. The use of diatomite as one of cement's ingredients has recently been shown to have positive effects. Moreover, diatomite is chemically inert to the majority of substances and has a very low thermal conductivity [25]. Özsoy et al. [26] investigated the impact of diatomite powder addition on the microstructural characteristics, mechanical strength, and high temperature resistance of fly ash-based geopolymer. The authors reported that the geopolymer mortar with 2% diatomite replaced had enhanced abrasion resistance and ultrasonic pulse velocity. Thammarong et al. [23] created geopolymer samples by substituting diatomite at the rates between 5% and 25% by weight of metakaolin for their research. They looked at the phase development of geopolymers activated with solutions of NaOH and Na_2SiO_3. The authors pointed out that compressive strength dramatically decreased at 25% diatomite content. This might be because the high concentration of silica from the diatomite weakens the sample's geopolymer network because the OH^- is unable to completely dissolve the Al^{3+} ions, leaving behind traces of the raw materials.

Andesite is classified as an igneous rock since it is a subspecies of igneous rocks Andesite is used in Turkey as well as other countries, especially for uses in civil engineering and architecture, including the creation of dripstone, parquet, frames, and cladding. Dust and aggregate are formed as a byproduct when natural stone is cut and polished for aesthetic uses. In the large-scale andesite production process, 70% of the andesite is lost during the mining, processing, and polishing stages, which generates a lot of waste. It has also been practiced to use waste andesite sand (AS) in mortars and concrete in place of cement or sand. The pozzolanic effects of waste andesite powder on the properties of high strength concrete were examined by Davraz et al. [27]. According to the authors, 10% was discovered to be the appropriate replacement rate of andesite waste powder for the C40 strength class for curing ages of 28 and 90 days. Celikten [28] investigated the properties of geopolymer mortars made from waste andesite dust involving the mechanical and microstructural characteristics. The findings revealed that higher flexural and compressive strength values may be determined using longer cure durations. In addition, the use of discarded andesite dust in geopolymer synthesis holds promise as an environmentally friendly and waste-free way to make mortar. The sludge waste generated during the cutting of andesite stones is stored in dust form after drying. The problem of waste storage is brought up by the variety of uses and consumption of andesite [29]. The originality of this study is to explore the potential for employing in alkali-activated composites to dispose of these wastes sustainably and recover value from them for the economy. The mechanical, durability and microstructural characteristics of alkali-activated composites made by substituting silica sand for waste andesite sand at weight ratios of 0%, 25%, 50%, and 100% were experimentally studied in the current work to achieve this goal. Natural pozzolans, which have a high silica and moderate alumina content and is widely available in volcanic regions, has been found as a sustainable alternative material for the production of alkali-activated or geopolymer binder.

It is well-known that the conventional concept of concrete is not a sustainable construction material solution, as it consumes natural resources both in the production of cement, its essential component, and in the production of the concrete itself. For this reason, researchers working in the field have been investigating the possibility of producing sustainable concrete. Alkali-activated composite is a relatively new concept that offers alternative construction material to conventional concrete since it consumes waste materials as binders instead of natural resources. However,

Table 1 Oxide composition of (% by mass) of GBFS and DP

Oxide	SiO_2	Al_2O_3	Fe_2O_3	CaO	MgO	Na_2O	K_2O	SO_3	LOI*
GBFS	32.3	16.9	0.8	39.5	8.3	0.4	0.6	< 0.1	< 0.1
DP	61.7	9.15	1.83	13.4	1.52	0.11	0.23	6.38	5.32

*Loss on ignition

the natural aggregate is still preferred in the production of this new concept. The aim of this study is to produce alkali-activated composites using not only waste powders but also waste aggregates to achieve a more sustainable approach to construction materials.

To the best of our knowledge, there has not been enough research done on the effects of waste andesite sand and diatomite powder on the microstructure, fresh, and durability properties of alkali-activated lightweight composites (AALC). GBFS and DP were used as the main solid precursors, SS and AS were used as fillers for the design of AALC mixtures. Sodium silicate and sodium hydroxide were chosen as the alkaline activators. Sixteen AALC mixtures were created using GBFS/DP ratios of 100/0, 90/10, 80/20 and 70/30 and AS was used to replace SS in four different proportions of 0%, 25%, 50%, and 100%. Prior to ambient curing, the manufactured samples were cured at 80 °C for 24 h to quicken geopolymerization. In addition to assessing its performance at freeze–thaw (F–T) cycles and high temperatures, physico-mechanical properties, transport properties, drying shrinkage, thermal conductivity, and sorptivity of produced AALC blends were also assessed. The microstructure of the AALC mixtures was also assessed using a scanning electron microscope (SEM).

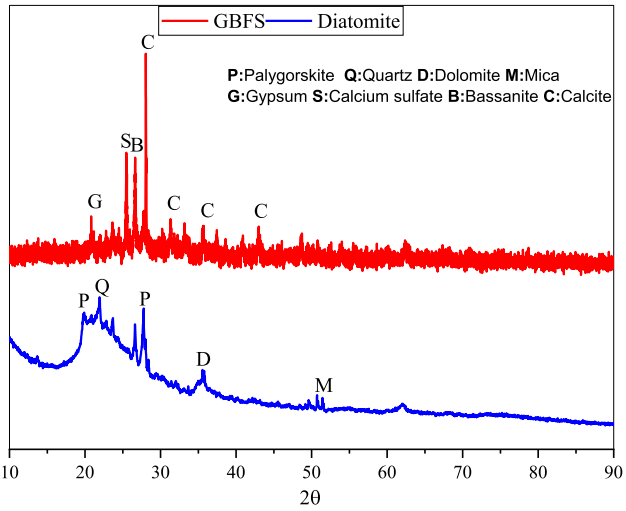

Fig. 1 XRD patterns of GBFS and DM

Table 2 Physical properties of silica and andesite aggregates

Properties	Silica aggregate	Andesite aggregate
Specific gravity	2.71	2.26
Water absorption (%)	3.23	5.78
Maximum particle size (mm)	2.36	2.36
Fineness modulus	2.87	2.74

2 Experimental program

2.1 Materials

GBFS and diatomite powder (DP), two binders with different chemical compositions, were employed in this investigation. The specific gravity and specific surface area (Blaine fineness) of GBFS are 2.87 and 4850 cm^2/g, respectively. The average particle size (d_{50}) of GBFS is 42 µm. In preparing the mixtures, DP was used as a precursor aluminosilicate material instead of GBFS at the rates of 0%, 10%, 20% and 30%. The specific gravity and specific surface area (BET) of DP are 2.03 and 12,300 cm^2/g, respectively. The chemical properties of GBFS and DP are presented in Table 1. The XRD analysis results for the mineral compositions of GBFS and DP are shown in Fig. 1. GBFS appears to have a high amorphous phase, as seen by the XRD pattern in Fig. 1. While GBFS comprised calcium carbonate ($CaCO_3$), calcium sulfate, bassanite ($2CaSO_4{\cdot}H_2O$) and gypsum ($CaSO_4{\cdot}2H_2O$) and, DP was composed of quartz crystal, palygorskite, gypsum ($CaSO_4{\cdot}2H_2O$) and dolomite ($CaMg(CO_3)_2$) crystalline phase.

This study was used silica sand (SS) with more than 95% SiO_2 content as aggregate. Andesite sand (AS) was used instead of silica aggregate at the rates of 0%, 25%, 50% and 100% at each DP content. The particle size of the aggregates is in the range of 0–2 mm. Other properties of silica and andesite aggregate are given in Table 2. To make the combinations more workable, a new generation polycarboxylate ether-based superplasticizer was employed. The superplasticizer (SP) had a solid content of 33% and the specific gravity is 1.12 ± 2.

In the fabrication of AALC mixtures, as alkali activators, sodium hydroxide and sodium silicate were selected. Sodium hydroxide is provided as white pellets, even though it is 99% pure. Tables 3 and 4 provide the technical characteristics of 12 M sodium hydroxide and sodium silicate,

Table 3 Properties of NaOH

NaOH	Na_2CO_3	Cl	SO_4	Fe	Al
99	0.3	< 0.01	< 0.01	< 0.01	< 0.01

respectively. For the mixes to be more workable, additional water from the tap was employed. For the purposes of the investigation, the consistency of the alkali-activated fresh concrete was provided by a super plasticizer (SP) concrete admixture based on polycarboxylate.

2.2 Mix design

In Table 5, the material quantity of the AALC mixtures created for the experimental investigation is listed. Sixteen mortar specimens were generated in which silica sand was replaced by AS in four ratios of 0%, 25%, 50% and 100% and DP replaced 0%, 10%, 20%, and 30% of the GBFS content. It was utilized to speed up the geopolymerization to cure at a temperature of 80 °C for 24 h.

2.3 Casting and curing of AALC mixtures

First, precursor aluminosilicate powders and aggregates were combined (2 min). The second stage involved adding NaOH to the liquid and mixing it for 2 min. After another 5 min, sodium silicate was added to the mixture. The 9-min-old geopolymer solutions have a fluid fluidity. After molding, fresh geopolymer mixes were put in the oven. Samples of geopolymer were cured in an oven that heated at a rate of 5 °C/min. It was used to quicken the geopolymerization process, so that it could cure for 24 h at 80 °C. The samples were stored in a curing room at a temperature of 25 °C and a humidity of 65% until the day of the test.

2.4 Testing

This study performed several experiments to look at the physical, mechanical, durability, and microstructural characteristics of mixes. Table 6 contains a list of the tests that were run, along with the sample sizes and test standards that were created for each test.

Table 4 Properties of Na_2SiO_3

Na_2O	SiO_2	H_2O	Specific gravity	Fe	Heavy metals	Appearance
8.8	28.2	63.0	1.38	< 0.01	< 0.01	Transparent

Table 5 Mixture proportions in AALC mixtures (kg/m^3)*

Mix ID	Andesite (%)	DP (%)	GBFS	DP	NaOH	Na_2SiO_3	Extra water	SP	Silica sand(SS)	Andesite sand(AS)
Ref	0	0	1000	0	90	210	175	50	496	0
D0A25	25	0	1000	0	90	210	175	50	372	124
D0A50	50	0	1000	0	90	210	175	50	248	248
D0A100	100	0	1000	0	90	210	175	50	0	496
D10A0	0	10	900	100	90	210	175	50	390	0
D10A25	25	10	900	100	90	210	175	50	293	98
D10A50	50	10	900	100	90	210	175	50	195	195
D10A100	100	10	900	100	90	210	175	50	0	390
D20A0	0	20	800	200	90	210	175	50	284	0
D20A25	25	20	800	200	90	210	175	50	213	71
D20A50	50	20	800	200	90	210	175	50	142	142
D20A100	100	20	800	200	90	210	175	50	0	284
D30A0	0	30	700	300	90	210	175	50	179	0
D30A25	25	30	700	300	90	210	175	50	131	48
D30A50	50	30	700	300	90	210	175	50	90	90
D30A100	100	30	700	300	90	210	175	50	0	179

*Mix ID (example): D10A50: D10: 10% DP–A50: 50% andesite

Table 6 Tests conducted, sample sizes and standards

Test	Standard	Sample size (mm)	Time (days)
Flow diameter	ASTM C1437 [30]	Fresh composites	
Apparent porosity	ASTM C642 [31]	50×50×50	28 days
Water absorption	ASTM C642 [31]	50×50×50	28 days
Hardened unit weight	ASTM C642 [31]	50×50×50	28 days
Flexural strength	ASTM C348 [32]	40×40×160	728 and 90 days
Compressive strength	ASTM C349 [33]	40×40×160	728 and 90 days
Freeze and Thaw resistance	ASTM C666 [34]	40×40×160	40, 80 and 120 cycles
Sorptivity	ASTM C1585 [35]	50×50×50	up to day 28
Drying shrinkage	ASTM C596 [36]	25×25×285	up to day 120
Thermal conductivity	ASTM D7984 [37]	20×50×100	28 days
High temperature		40×40×160	300–600–900 °C

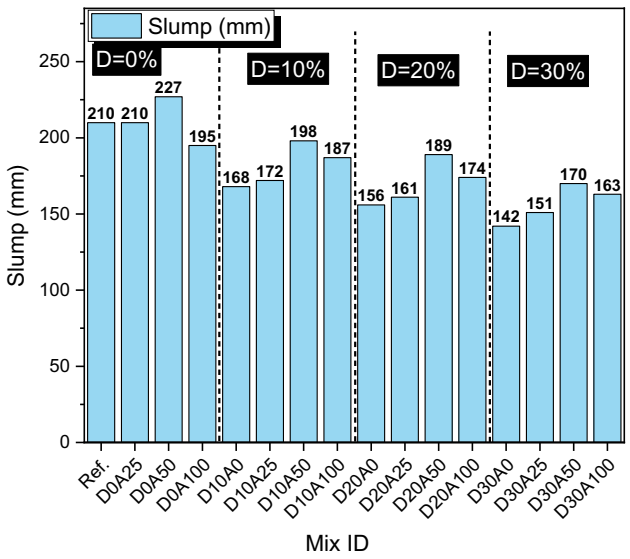

Fig. 2 Slump values of AS and DP incorporated AALC mixtures

3 Results and discussion

3.1 Consistency of AALC mixtures

Figure 2 shows the impact of DP as a precursor and andesite sand as a fine aggregate on the consistency (slump) of AALC mixtures. The slump values for all AALC mixtures ranging from 227 to 142 mm are illustrated in Fig. 2. The mixture without DP(D = 0%) exhibited slump values unchanged and then gained the greatest slump value of 227 mm at 50% AS content, and then the slump value decreased at 100% AS content. It is clearly seen from Fig. 2 that at each DP content, slump values increased by replacing SS with 25% and 50% AS but a light decrease was seen at 100% AS content. The mixture with 50% AS showed the highest slump value at each DP content, and the mixture with no AS showed the lowest slump value at each DP content. When the AS in the AALC mix was increased to 100%, it was discovered that the slump flow of AALC mixture decreased by as much as 7.14% at 0% DP content when compared to reference mix. It was found that the slump flow of the AALC mixture improved by as much as 11.30%, 11.53% and 14.78% when the AS in the AALC mix was increased to 100% at 10%, 20% and 30% DP content, respectively, as compared to the mixture without AS. Fresh AALC mixtures with AS showed less cohesive and more workable than AALC mixtures made of SS. With the addition of AS instead of SS, the increase in slump values, especially in mixtures containing DP, can be attributed to the form, surface morphology and particle size distribution of AS. In addition, according to the ASTM C33 standard, the fineness modulus of AS was significantly lower than SS. Replacing GBFS with DP decreased the flowability of fresh AALC mixtures. Because there is more diatomite powder in the mortar mixture, the flow value has decreased. Due to the exceptional fineness and specific surface area of diatomite powder, the flow value of the cement mortar containing it is significantly reduced. This is mainly due to that increasing the diatomite amount in the mixture results in the agglomeration of particles and reduces workability [26].

In comparison with GBFS, diatomite powder had a specific surface area that was around 2.5 times greater and a 29% lower specific gravity. DP absorbs water significantly more than GBFS because of its higher specific surface area and lower specific gravity; therefore, the fluidity of AALC mixtures containing diatomite is significantly reduced with increasing DP content. The diatom frustules' (empty, perforated sheaths) morphology actually swallowed the mixing water with extremely strong capillary suction forces [38, 39]. When the DP in the AALC mixture without AS was increased to 10%, 20%, and 30%, it was discovered that the slump flow reduced by as much as 20.00%, 25.71%, and

32.38%, respectively, when compared to the mixture without AS and 0% DP content.

3.2 Compressive strength

Figure 3 reports the compressive strength development of produced mixtures containing DP as a precursor and andesite sand as a fine aggregate cured for 7, 28 and 90 days. Figure 3a shows the compressive strength of the mixtures containing 0% and 10% DP as a substitute of GBFS and Fig. 3b presents the compressive strength of the mixtures containing 20% and 30% DP as a substitute of GBFS. The compressive strength containing AS and 0% DP mixtures ranged from 43.50 to 46.97 MPa at 7 days, 45.17 to 55.06 MPa at 28 days, and 50.39 to 59.95 MPa at 90 days. When considered the compressive strength development of AALC mixtures with 0% DP content, the findings showed that during all curing times, compressive strength of AS incorporated AALC mixtures was greater than the reference mixture as given in Fig. 3a. It can be noticed that replacing AS with SS improved the compressive strength with increasing AS content. After 28 days, the compressive strength for D0A25, D0A50, and D0A100 increased by 12.90%, 13.37%, and 21.89%, respectively, in comparison with the reference mixture. After 90 days, D0A25, D0A50, and D0A100 all had compressive strengths that were higher than the reference mixture by 7.84%, 10.47%, and 18.97%, respectively. The fineness of the AS particles, which had the right gradient and shape to fill the pores and improve the pore structure, is primarily responsible for this increase in compressive strength. Furthermore, the coarse and angular texture of AS materials improved bonding between the slag and aggregate interfaces, resulting in the high strength. The ITZ between the biggest sand particles and the geopolymeric matrix, which is where this phenomenon is most likely to occur, can be considered. The compression strength findings are consistent with earlier investigations [27, 28, 40]. The strength of AALC mixtures improved as the proportion of AS grew, with the substitution of AS for SS up to 100% being advantageous for making AALC due to the absence of strength deterioration for the mixtures without DP. AALC samples without DP cast with 100% AS substitute instead of SS, on the other hand, demonstrated best strength throughout the curing process and were thus selected as the best mixture. However, replacing GBFS with DP as a precursor at the rates of 10%, 20% and 30% decreased the compressive strength significantly especially at the 20% and 30% DP replacement ratios regardless of AS content. After 28 days, the compressive strength for D10A0, D10A25, D10A50, and D10A100 decreased by 3.82%, 12.88%, 11.50%, and 21.35%, respectively, in comparison with the corresponding mixtures without DP (i.e., Ref., D0A25, D0A50, and D0A100). After 90 days, the compressive strength of D10A0, D10A25, D10A50, and D10A100 reduced by 9.58%, 15.99%, 12.01%, and 20.51%, respectively, as compared to the same mixtures without DP (i.e., Ref., D0A25, D0A50, and D0A100). The reduction results showed that greater strength loss was seen for the AALC mixtures without AS and lower AS content of 25% at later curing ages. At greater content of AS, reduction remained almost unchanged at 90 days. Similar but more strength reduction with replacing GBFS with 20% and 30% DP can also be observed, as clearly shown in Fig. 3b. The

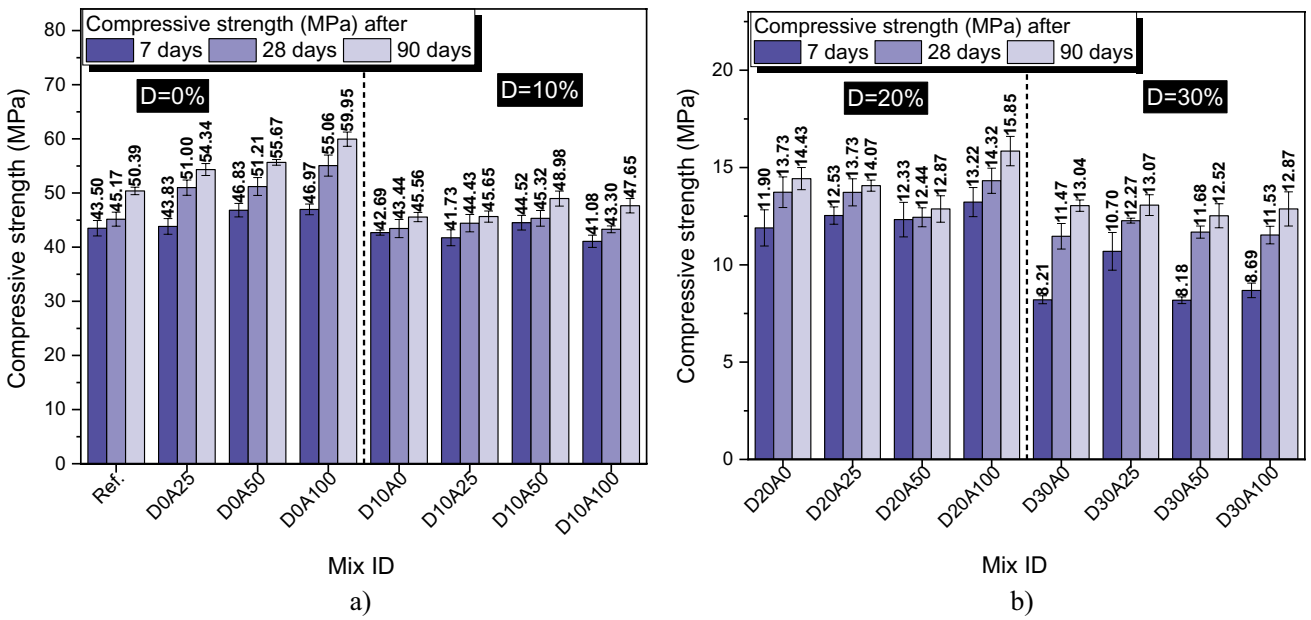

Fig. 3 Outcomes of compressive strength at **a** DP = 0% and 10% and **b** DP = 20% and 30%

increase in the pores and porosity of AALC structure due to the broken and highly micro porous structure of DP particles resulted in the compressive strength reduction. This might also be because there is a lot of silica in the sample owing to the diatomite, which reduces the compressive strength of the geopolymer network because the OH^- is not strong enough to completely dissolve the Al^{3+} ions, leaving behind undissolved raw materials that weaken the sample [23]. Furthermore, although the slag combination reacts to form a C–(A)–S–H-like gel under moderately alkaline conditions, lower reactivity of DP weakened bonding between the slag and aggregate interfaces in the geopolymeric matrix, resulting in the lower strength [41]. Diatomite is being studied by Degirmenci and Yilmaz [41] as a possible partial cement replacement in cement mortar manufacture. The results of experiments on compressive and flexural strength, water absorption, sulfate resistance, and freeze–thaw resistance led the authors to suggest using diatomite up to 5% instead of Portland cement.

3.3 Flexural strength

Figure 4 shows the flexural strength development of produced mixtures containing DP as a precursor and andesite sand as a fine aggregate cured for 7, 28 and 90 days. In Fig. 4a, the mixtures with 0% and 10% DP as a substitute for GBFS are depicted with their flexural strengths and the flexural strength of the mixtures including 20% and 30% DP as a replacement for GBFS is shown in Fig. 4b. For mixes including AS and 0% DP mixtures, the flexural strength ranged from 3.05 to 3.14 MPa at 7 days, 3.15 to 3.40 MPa at 28 days, and 3.21 to 3.53 MPa at 90 days. When the flexural strength of AALC mixtures with 0% DP content was taken into account, the results revealed that flexural strength of AS integrated AALC mixtures was slightly lower than the reference mixture, as shown in Fig. 4a, during all curing durations. When AS was substituted for SS, the flexural strength decreased by AS content increased. After 28 days, D0A50, and D0A100 all had flexural strengths that were lower than the reference mixture by 4.47% and 5.97%, respectively, but D0A25 exhibited slightly greater than reference mixture. After 90 days, the flexural strengths of D0A25, D0A50, and D0A100 were all lower than the reference mixture by 1.98%, 8.50%, and 9.06%, respectively. The reduction rates after 90 days showed that more flexural strength loss was recorded at 50% and 100% AS content. The increase in porosity of the AALC mixture with an increasing content of AS could be the primary explanation for the reduction in flexural strength caused by the substitution of SS with AS. In contrast, regardless of AS content, replacing GBFS with DP as a precursor at rates of 10%, 20%, and 30% also reduced flexural strength. After 28 days, the flexural strengths of D10A0, D10A25, D10A50, and D10A100 were all lower than those of the corresponding mixtures without DP (i.e., Ref., D0A25, D0A50, and D0A100) by 11.04%, 13.52%, 9.68%, and 14.92%, respectively. Comparing the flexural strength of the same mixtures without DP (i.e., Ref., D0A25, D0A50, and D0A100) after 90 days, D10A0, D10A25, D10A50, and D10A100 each experienced a reduction of 12.46%, 9.82%, 7.43%, and 14.01%, respectively. As shown in Fig. 4b, a similar but greater strength loss is also exhibited when GBFS is replaced by 20% and 30% DP. It seems that more flexural

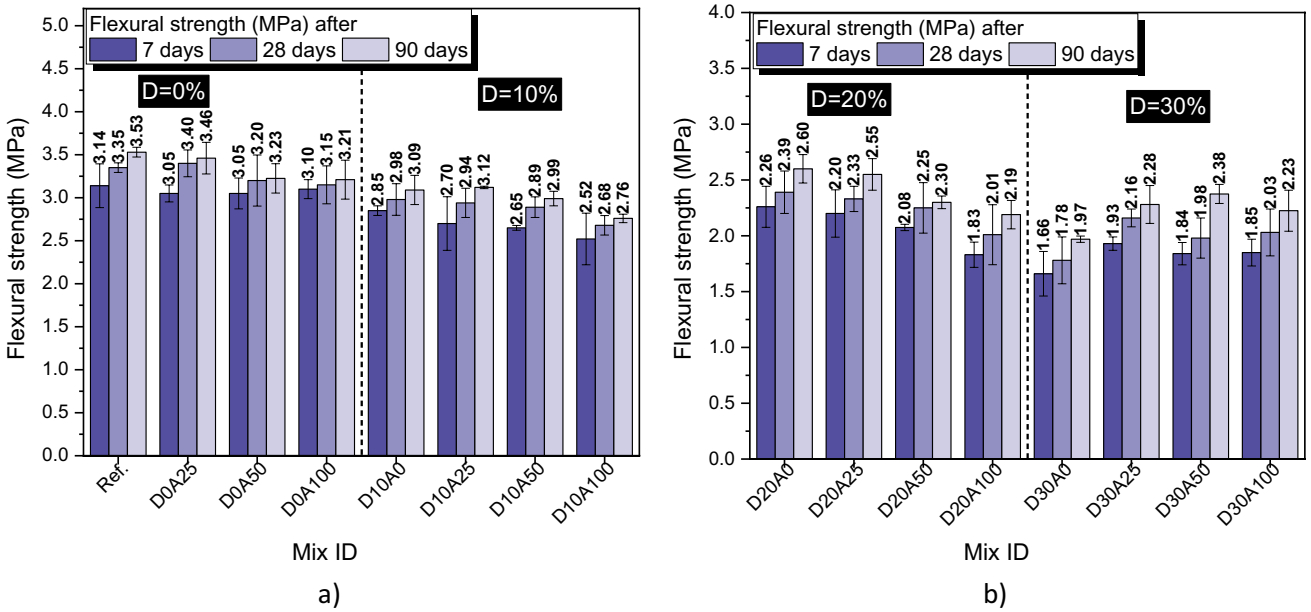

Fig. 4 Outcomes of flexural strength at **a** DP = 0% and 10% and **b** DP = 20% and 30%

strength decrease was measured with increasing AS content 0%, 10% and 20% incorporating AALC mixtures but at 30% DP content, flexural strength increased with increasing AS content. The aggregation of diatomite particles and decrease in workability values account for the loss of strength in the outcomes of compression and flexure. Since increasing rate of diatomite is replaced by fly ash, this creates agglomeration in the mixture, which lowers the workability value and results in improper compaction during the sample casting process, which lowers the flexural and compressive strength [26].

3.4 Dry unit weight

Figure 5a illustrates how the addition of andesite sand as a fine aggregate and DP as a precursor affected the dry unit weight of 28-day ambient cured AALC mixtures. The dry unit weight containing AS and 0% DP–AALC mixtures ranged from 1776 to 1817 kg/m^3. As shown in Fig. 5a, the AALC mixtures without DP as a substitute of GBFS exhibited greater unit weight than the mixtures containing 10%, 20% and 30% DP. The greatest dry unit weight was seen for the mixtures without DP. Replacing GBFS with DP led to decrease in dry unit weight of AALC mixtures and the lowest dry weight was seen for the mixtures containing 30% DP. Replacing SS with AS showed no much change in unit weight only slight increase or decrease of about 3% depending on DP content. When considered the effect of DP on dry unit weight, the greatest reduction in dry unit weight was determined as 17.17% for the greatest dry unit weight and the lowest dry unit weight. Since DP have lower specific gravity than GBFS and have a high porosity, and a big pore volume due to the significant number of small microscopic pores, adding DP instead of GBFS increased the pores and porosity of the AALC mixtures leading to the dry unit weight reduction. Phoo-ngernkham et al. [42] investigated the effects of diatomite addition on the characteristics of high calcium fly ash geopolymer pastes and showed also that the unit weight tended to decrease as diatomite content increased. The relationship between the unit weight and compressive strength of AALC mixtures is shown in Fig. 5b. The correlation factor R^2 between the compressive strength and unit weight of AALC mixtures was found to be the value of 0.92. It has been stated that mechanical properties of cement or alkali-activated-based materials are strongly dependent of the physical and transport properties of mentioned materials if many different parameters do not exist in the materials [12]. In the study by Kearsley and Wainwright [43], the porosity has been proven to be largely dependent on the dry density. In addition, compressive strength has been determined as a function of porosity and age. Similar relationships were also reported in our previous studies related to the cement and alkali-activated-based composites [11, 44, 45].

3.5 Thermal conductivity

The effect of using andesite sand as a fine aggregate and DP as a precursor on the thermal conductivity of AALC mixtures after a 28-day curing period in the ranges of 0.73 to 1.55 (W/mK) is shown in Fig. 6a. Porosity, concrete density, and cement matrix are significant variables that have a direct impact on thermal conductivity. As a result, identical findings to those of previous investigations were

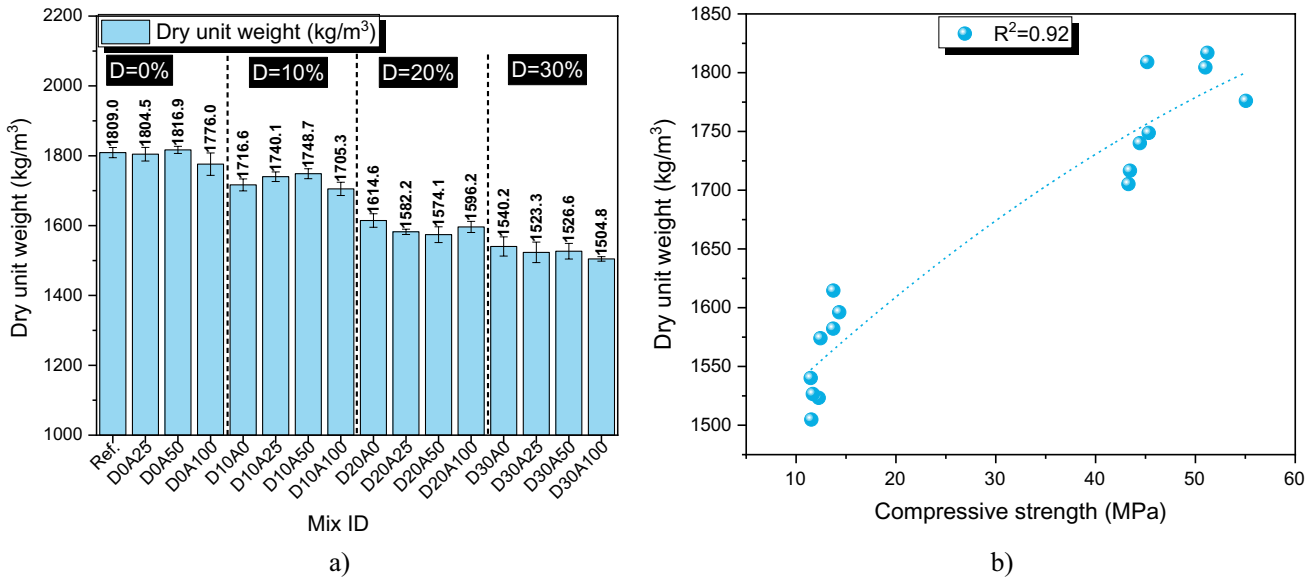

Fig. 5 Outcomes of unit weight **a** dry unit weight vs. the compressive strength **b**

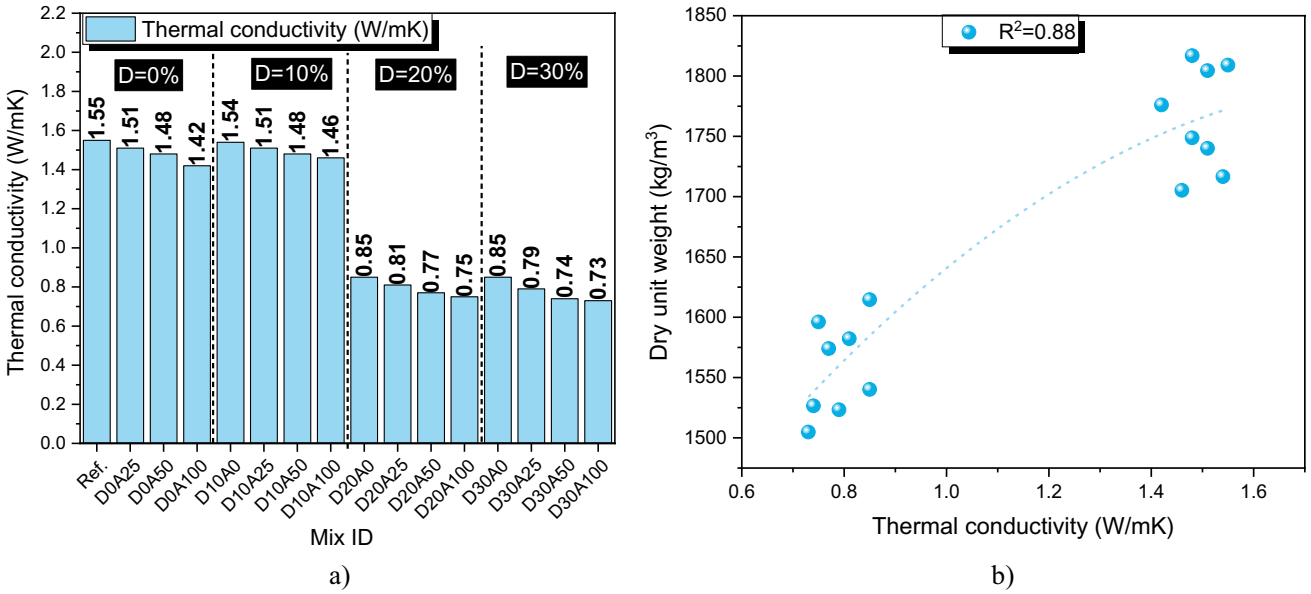

Fig. 6 Outcomes of thermal conductivity **a** thermal conductivity vs. dry unit weight **b**

found in this study, which indicated that thermal conductivity declined as porosity and dry unit weight enhanced [46–50]. With the mixture D30A100 reaching the lowest thermal conductivity value, it is clear that using DP in place of GBFS considerably increased porosity and decreased thermal conductivity. The fragmented and extremely micro porous structure of the DP particles, which increased the holes and porosity of the AALC structure, was primarily responsible for this increase in porosity. Lower specific gravity, as previously stated, also contributed to this rise in porosity and decrease in thermal conductivity. It could be explained by the fact that AALC samples with DP incorporation show less geopolymerization or produce hydration products with lower hydration, resulting in larger porosity and lower thermal conductivity. Since diatomite is a common biological mineral element found in aquatic diatom skeletons. It has a sophisticated structure with a large number of small microscopic pores that are evenly distributed, high porosity, and a large pore volume and lower thermal conductivity [51]. Replacing SS with AS also showed slight decrease in thermal conductivity values. The relation between unit weight and thermal conductivity after 28 days of curing is shown in Fig. 6b. In the relationship between unit weight and thermal conductivity for AALC mixtures, the correlation factor R^2 was observed to have a very strong value of 0.88. Dry unit weight improved with increasing thermal conductivity. The literature is consistent with the significant correlation found between the dry unit weight and thermal conductivity of the cement and alkali-activated-based composites [12, 52, 53]

3.6 Assessment of porosity and water absorption

Figure 7a shows the impact of DP as a precursor and andesite sand as a fine aggregate on the porosity and water absorption of AALC mixtures cured for 28 days. That has to be highlighted that the relationship between dry unit weight and porosity is inverse, meaning that the higher the dry unit weight of the composite, the lower the porosity. The porosity comprising AS and 0% DP–AALC mixtures ranged from 20.9% to 24.5%. The porosity including 10% DP–AALC mixes and AS varied from 23.5% to 25%. The 20% DP–AALC and AS mixes' porosities ranged from 31.0% to 32.1%. The porosity containing AS and 30% DP–AALC combinations ranged from 33.0% to 35.2%. It is obvious that using DP in place of GBFS greatly increased porosity and water absorption, with the mixture D30A50 achieving the highest values. This increase in porosity and water absorption was mostly related to the fractured and very micro porous structure of DP particles, which enhanced the pores and porosity of the AALC structure. As it was expressed before lower specific gravity also caused this increase porosity and water absorption. It may be explained by the fact that, DP-incorporated AALC samples exhibit less geo-polymerization or produce lower hydration products leading to higher porosity. Due to its large specific area and porous nature, diatomite inclusion in cement mortar (over 15%) slightly improves the moisture storage [41]. Since Diatomite is a common biological mineral element that forms the skeleton of aquatic diatoms. It features a complicated structure with a large number of regularly distributed fine microscopic pores, high porosity, and a big pore volume

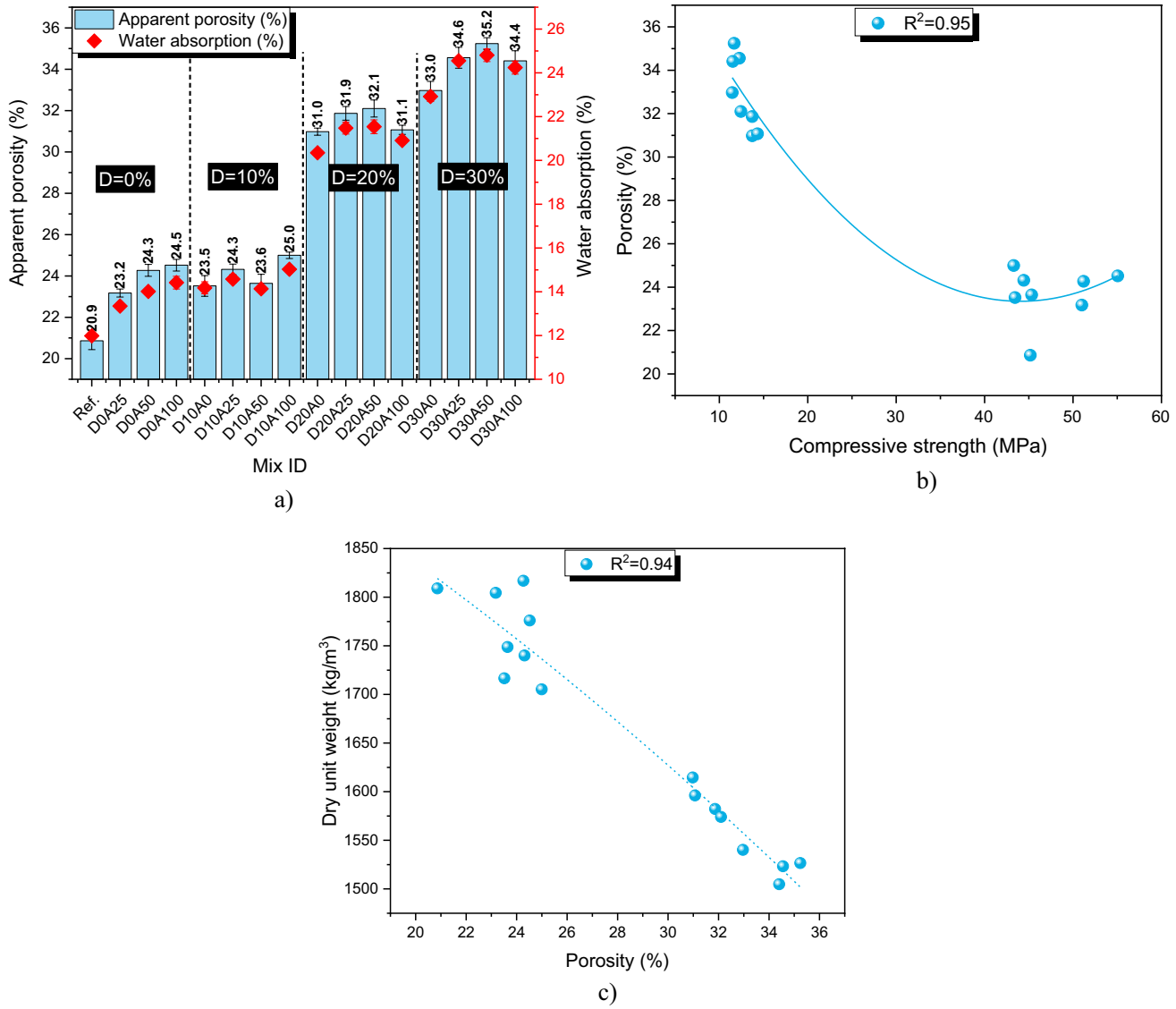

Fig. 7 Water absorption and porosity **a** compressive strength vs. porosity **b,** porosity vs. the unit weight **c**

[51]. Replacing SS with AS showed no much change, only slight increase or decrease in porosity and water absorption values depending on AS content especially at 20% and 30% DP content in which the mixtures with 50% AS exhibited the higher values. The results obtained from the effect of AS on the porosity and water absorption were consistent with the study conducted by Davraz et al. [27]. The water absorption of the combinations varied in direct proportion to the porosity values, as shown in Fig. 7b. It should be noted that a linear regression R^2 of 0.95 may be obtained for the correlation between the compressive strength and porosity of AALC mixtures. When looking at the association between porosity and dry unit weight in Fig. 7c, the correlation factor R^2 of 0.94 was determined. The porosity has been shown in the work by Kearsley and Wainwright [43] to be primarily dependent on the dry density. In addition, it has been established that porosity and age affect compressive strength. Similar relationships were also noted in our earlier research on composites made of cement and with alkali activator [11, 44, 45, 50].

3.7 Evaluation of drying shrinkage

The effect of andesite sand as a fine aggregate and DP as a precursor on the drying shrinkage of AALC mixtures for a 120-day drying period is shown in Fig. 8a. The drying shrinkage of AALC mixtures develops first 28 days, then declines until it reaches a stable level, lengthening the drying time even further. Shrinkage behavior and control methods of AALC are extensively established. When compared to

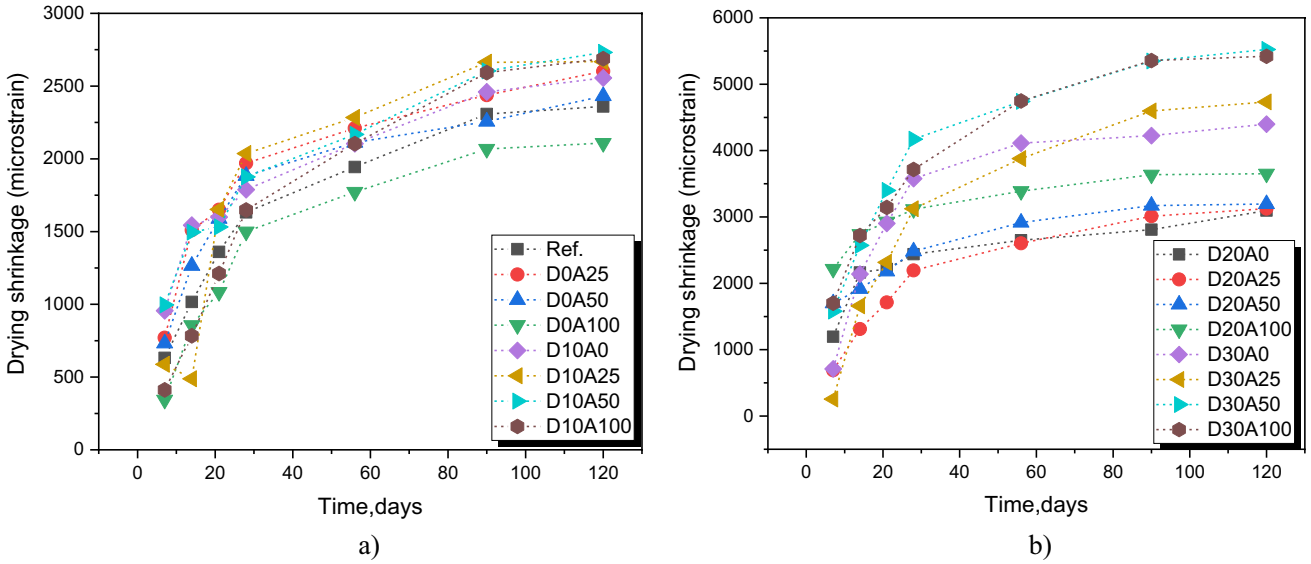

Fig. 8 Drying shrinkage results at **a** DP = 0% and 10% and **b** DP = 20% and 30%

Portland cement, AALC shrinks excessively. The fundamental explanation is the increased capillary force caused by the alkali activator's refining of the pore size in the material. In terms of drying shrinkage, because there is more free water in AALC in the inner pores of the gel than when it is included with hydration products, water loss of this area causes evident drying shrinkage [54–56]. Evidently, the addition of DP significantly increased the shrinking of the specimens throughout drying durations, as shown in Fig. 8a, b. Since compressive strength development has a large impact on shrinkage, this enhancement may be caused by a decrease in compressive strength as a result of a rise in DP content. Addition of AS instead of SS also increased the shrinkage values especially at the content of 20% and 30% DP incorporated AALC mixtures. The AALC mixtures without DP showed the lowest shrinkage values in all mixtures. D0A100 exhibited the lowest dry shrinkage of 2108 micro strain with a reduction of 10.68% in comparison with reference mixture at the end of drying period. Addition of 100% AS instead of SS affected the shrinkage positively and had a positive effect on reducing shrinkage for the mixtures without DP. On the other hand, the 10% DP incorporated AALC mixture with 50% AS revealed the highest shrinkage and the mixture without AS showed the lowest shrinkage at this DP content. As is evident in Fig. 8b, replacing GBFS with 20 and 30 DP significantly reduced the shrinkage resistance of AALC mixes. Due to the loose nature of diatomite and the abundance of small pores, micro pores form when the diatomite piece shrinks at a high temperature. It is obvious that adding diatomite has a big impact on porosity [51]. When compared the shrinkage values of the AALC mixtures containing 30% DP with the AALC mixtures without DP, the shrinkage values for D30A0, D30A25, D30A50, and D30A100 increased by 86.35%, 81.86%, 127.14%, and 157.11%, respectively, in comparison with the corresponding mixtures without DP (i.e., Ref., D0A25, D0A50, and D0A100).

3.8 Sorptivity

Sorptivity is a crucial factor in determining how long AALC and geopolymer binders will last. The main reason why concrete degrades throughout the course of its life is because carbonates and sulphate get inside through capillary pores. The sorptivity test is just one of the numerous methods used to gauge the permeability properties of concrete. Figure 9 shows the impact of DP as a precursor and andesite sand as a fine aggregate on the sorptivity of AALC mixtures for up to 28 days. It is apparent in Fig. 9, sorptivity of AALC mixtures increased sharply in the first period then gained a stable level and remained unchanged. As shown in Fig. 9a, b, it is clear that adding DP greatly increased the sorptivity of AALC specimens during the test period. Given the significant influence that compressive strength development has also on sorptivity, this enhancement in sorptivity could be brought about by a decline in compressive strength as a result of an increase in DP content. Depending on the amount of DP added, using AS instead of SS has an impact on the sorptivity either favorably or unfavorably. The AALC mixture without DP and containing 100% AS (D0A100) showed the lowest sorptivity value of 11.76 mm/s$^{0.5}$ by 14.65% reduction with respect to the 28-day ambient cured reference mixture. The mixture with the lowest sorptivity also exhibited the highest compressive strength as already mentioned. On

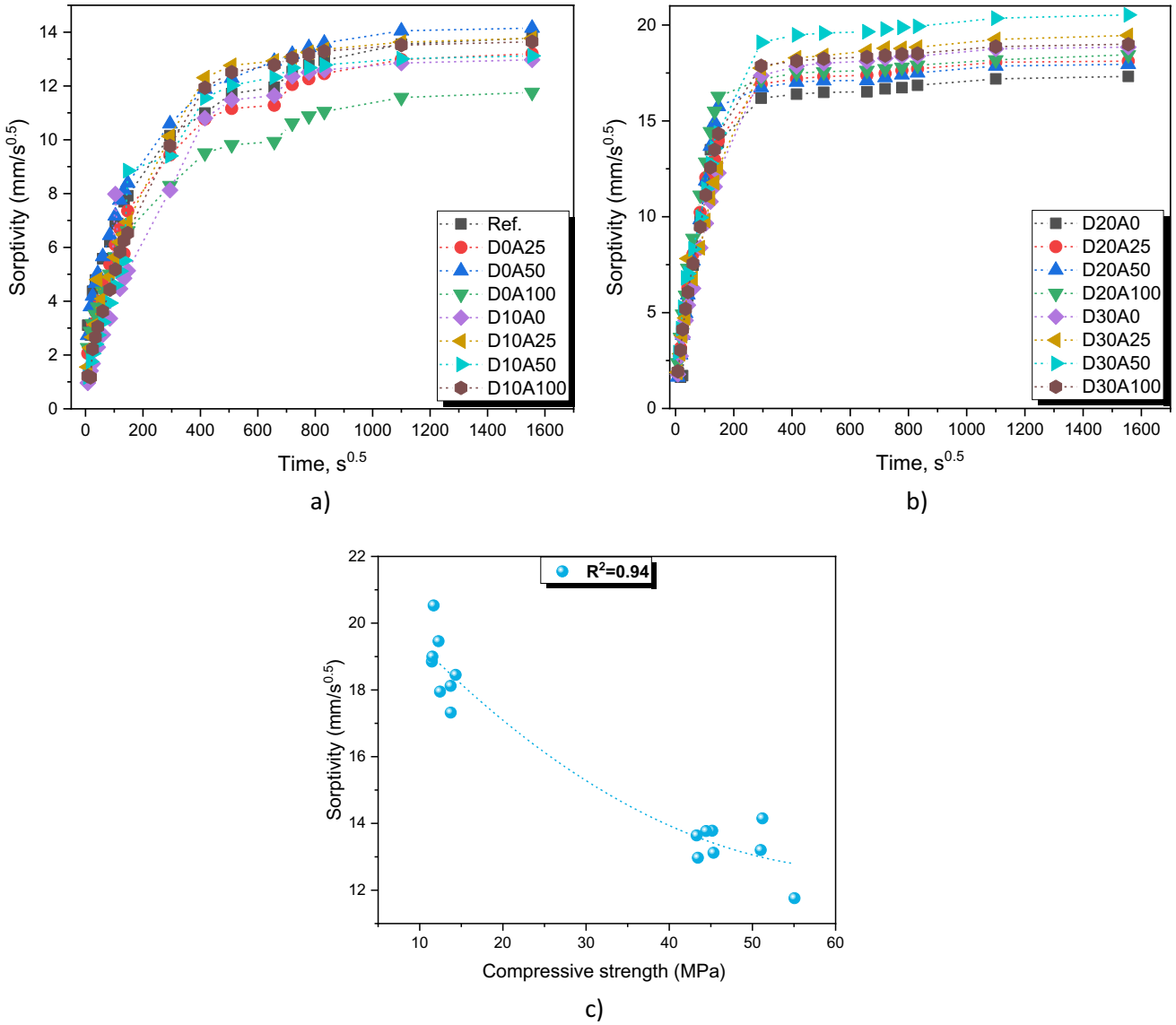

Fig. 9 Sorptivity results at **a** DP = 0% and 10%, **b** DP = 20% and 30%, **c** compressive strength vs. sorptivity

the other hand, the mixture with 25% AS showed the highest sorptivity at this DP content, while the mixture with 10% DP included AALC showed the lowest sorptivity. The sorptivity of the other mixtures with AS actually did not vary much that much. As can be seen in Fig. 9b, adding 20 and 30 DP instead of GBFS enhanced the sorptivity of AALC mixes. It is clear that including diatomite has a significant effect on porosity [51] leading to enhancement in sorptivity. When compared the sorptivity values of the AALC mixtures containing 30% DP with the AALC mixtures without DP, the sorptivity values for D30A0, D30A25, D30A50, and D30A100 increased by 36.79%, 47.42%, 45.08%, and 161.56%, respectively, in comparison with the corresponding mixtures without DP (i.e., Ref., D0A25, D0A50, and D0A100). As shown in Fig. 9c, the relationship between the sorptivity and compressive strength of AALC mixtures was found to have an R^2 value of 0.94. It appears that sorptivity and compressive strength are related, with more sorptivity being associated with lesser compressive strength.

3.9 Microstructural properties of heat-cured mixtures

The microstructure properties of the reference mixture at different magnifications are presented in Fig. 10. It has been determined that spherical air voids are formed in the matrix and these voids are generally smaller than 10 µm. In addition, it is seen that the adhesion of the aggregate with the paste is quite good. Because the interface between paste and aggregate is quite dense, the micro cracks rate is very low. It

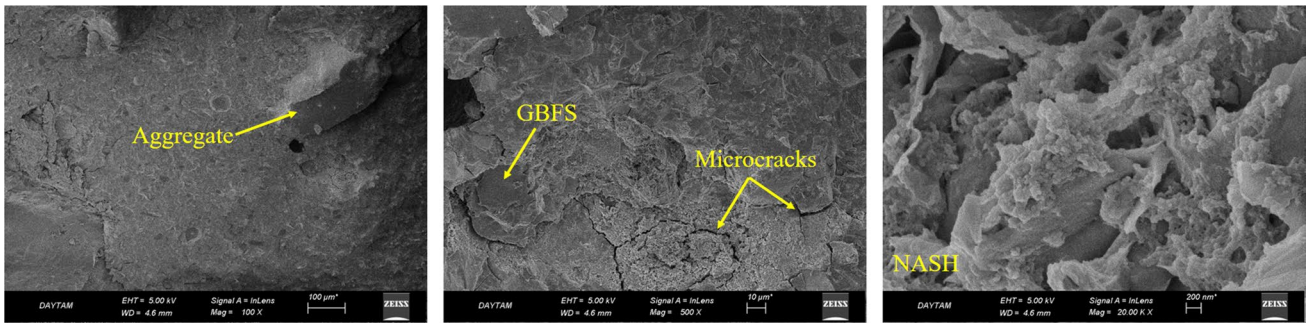

Fig. 10 Microstructure images of reference mix cured for 90 days

is thought that the micro cracks in the matrix are caused by the thermal cure applied at 80 °C. Such a network of micro cracks was observed in some parts of the matrix. In addition, GBFS grains embedded in the matrix but not hydrated were determined. It has been determined that the matrix is quite dense in the reference mixture with a compressive strength of 50 MPa. As a result of the reaction of GBFS with alkaline solutions in the matrix, nanoscale N–A–S–H gel was formed.

The matrix of the 90-day-cured D10A50 mixture had air voids with a diameter of around 10 µm (Fig. 11.). It has been determined that these cavities are generally spherical in shape. It is also thought that these voids originate from the polycarboxylate-based superplasticizer. It has been determined that a micro crack network is formed in the matrix. These cracks are shrinkage cracks formed during thermal curing. However, it was discovered that the silica sand cracks appeared following the compressive strength test. In SEM examinations, it was observed that the interface between paste–aggregate was quite dense. Already in the D10A50 mixture, compressive strength of about 50 MPa was obtained on the 90th day. This is proof that the aggregate–paste interface is dense. In the matrix, a dense N–A–S–H gel was also discovered. This gel was formed due to the activation of GBFS and DP with alkaline solutions.

Figure 12 shows SEM pictures of the D30A100 mixture after 90 days of curing, at a compressive strength of around 13 MPa. Since the compressive strength is low, micro cracks were observed in the interfacial transition zone between the paste–aggregate. As in other mixtures, spherical air bubbles were determined in the D30A100 mixture. Although the DP ratio was 30%, nanoscale N–A–S–H gels were detected in the matrix. Although it was observed that the matrix was dense in some regions, DP with a low degree of amorphism decreased the compressive strength. The resulting N–A–S–H gels are generally thought to originate from GBFS.

3.10 High-temperature resistance

It was determined how resistant AALC mixes were to high temperatures at 300 °C, 600 °C, and 900 °C. This was heated at a rate of 5 °C. The samples were exposed to a heated atmosphere for 2 h. The samples were then gradually cooled to room temperature. High temperature resistance will be analyzed using mechanical properties and mass loss.

3.10.1 Compressive strength

Figure 13a, b illustrates how andesite sand, used as a fine aggregate, and DP, used as a precursor, affected the average

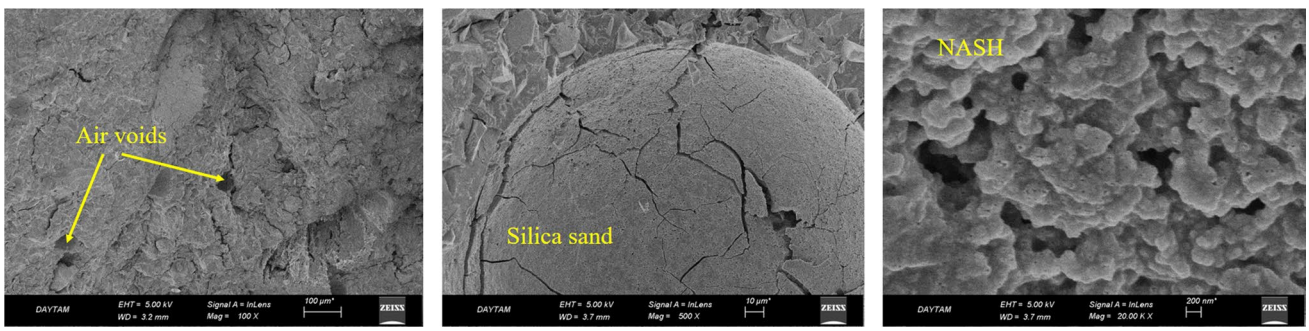

Fig. 11 Microstructure images of D10A50 mix cured for 90 days

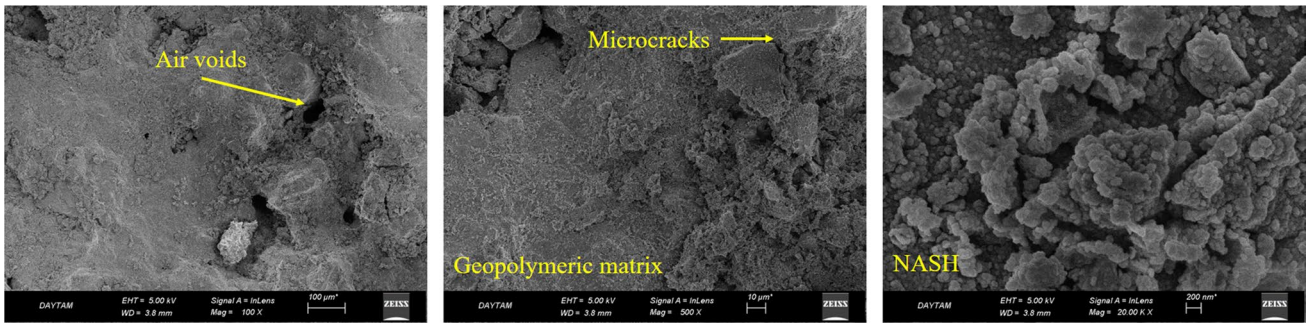

Fig. 12 Microstructure images of D30A100 mix cured for 90 days

compressive strength of AALC mixes at high temperatures. Figure 13c, d illustrates how compressive strength changes while being exposed to high temperatures. As shown in Fig. 13, all AALC mixtures exhibited compressive strength enhancement after 300 °C exposure. This enhancement can be attributed to the more geopolymerization resulting from GBFS and DP unreacted particles that encourage the development of C–S–H minerals to develop a higher strength at this temperatures [57]. The heating procedure also causes the creation of vapor and "internal autoclaving," which encourages more hydration and consequently increases chemical boundaries. The high-temperature resistance of AALC mixtures was greatly improved when GBFS was replaced with DP, notably at 20% and 30% DP content. At 0% DP content, the highest strength enhancement was measured for the reference mixture with the strength increase of 30.2% and the second best resistance to high temperature with strength increase of 26.9% was seen for the mixture with 50% AS (D0A50) at 300 °C. The mixture with 50% AS (D0A50) also exhibited the best resistance to elevated temperature of 600 °C with the strength enhancement of 15.1% and the same mixture showed the lowest strength loss of 66.7% among the mixtures without DP. At 10% DP content, the mixture without AS (D10A0) had the highest strength enhancement, with a strength increase of 29.0% and 1.5% after 300 °C and 600 °C, respectively. While the same mixture demonstrated the least amount of strength loss, 69.3%, among mixtures 10% DP after 900 °C. It appears that the strength improvement at 300 °C with increasing content was lessened at this DP content by the introduction of AS. As denoted in Fig. 13, the mixture D10A25 performed the worst after high temperatures of 600 and 900 °C among 10% DP incorporated AALC mixtures. At 20% DP content, more positive effect of addition AS was observed for all temperature ranges. The mixture D20A50 (containing 20% DP and 50% AS) exhibited compressive strength enhancement significantly by 59.4% and 22.2% at 300 °C and 600 °C, respectively, and also showed the lowest strength loss of 20.7% at 900 °C among all AALC mixtures regarding the DP and AS content. The mixture D20A100 performed the worst after high temperatures of 900 °C among 20% DP incorporated AALC mixtures. Due to their lower thermal expansivity value and higher thermal stability under high temperatures, lightweight aggregates were stated to produce lightweight concretes that exhibit better fire resistance than standard concretes [58–62]. The explanation for the improvement in mechanical characteristics with increased DP and AS content can also be attributed to the increase in porosity during thermal curing and the increase in porosity producing more geopolymerization and hydration products at higher temperatures. As clearly seen from Fig. 13d, the mixtures containing 20% and 30% DP revealed excellent high temperature resistance while comparing with the mixtures with 0% and 10% DP. More strength enhancement was observed at 300 °C and 600 °C and less decrease in strength reduction was determined at 900 °C. At 30% DP content, more compressive strength enhancement was seen and the increments were 26.1%, 45.1%, 66.0% and 55.0% at AS contents of 0%, 25%, 50% and 100% at 300 °C, respectively. When considering the high temperature effect of 900 °C, the mixture containing 100% AS (D30A100) exhibited the best performance and the lowest strength reduction of 22.3%. These results can be explained by the fact that high specific surface area, substantial absorbability, and remarkable thermal and chemical stability of DP at high temperatures [63].

3.10.2 Flexural strength

As denoted in Fig. 14a, b, the influence of andesite sand as a fine aggregate and DP as a precursor on the mean flexural strength of 28-day ambient cured AALC mixtures while being subjected to high temperatures. Figure 14c, d depicts the change in flexural strength under high temperatures. All AALC mixtures demonstrated increased flexural strength after being exposed to 300 °C, similar to compressive strength performance, as shown in Fig. 14. The increased geopolymerization caused by the GBFS and DP unreacted particles, which encourage the synthesis of C–S–H minerals

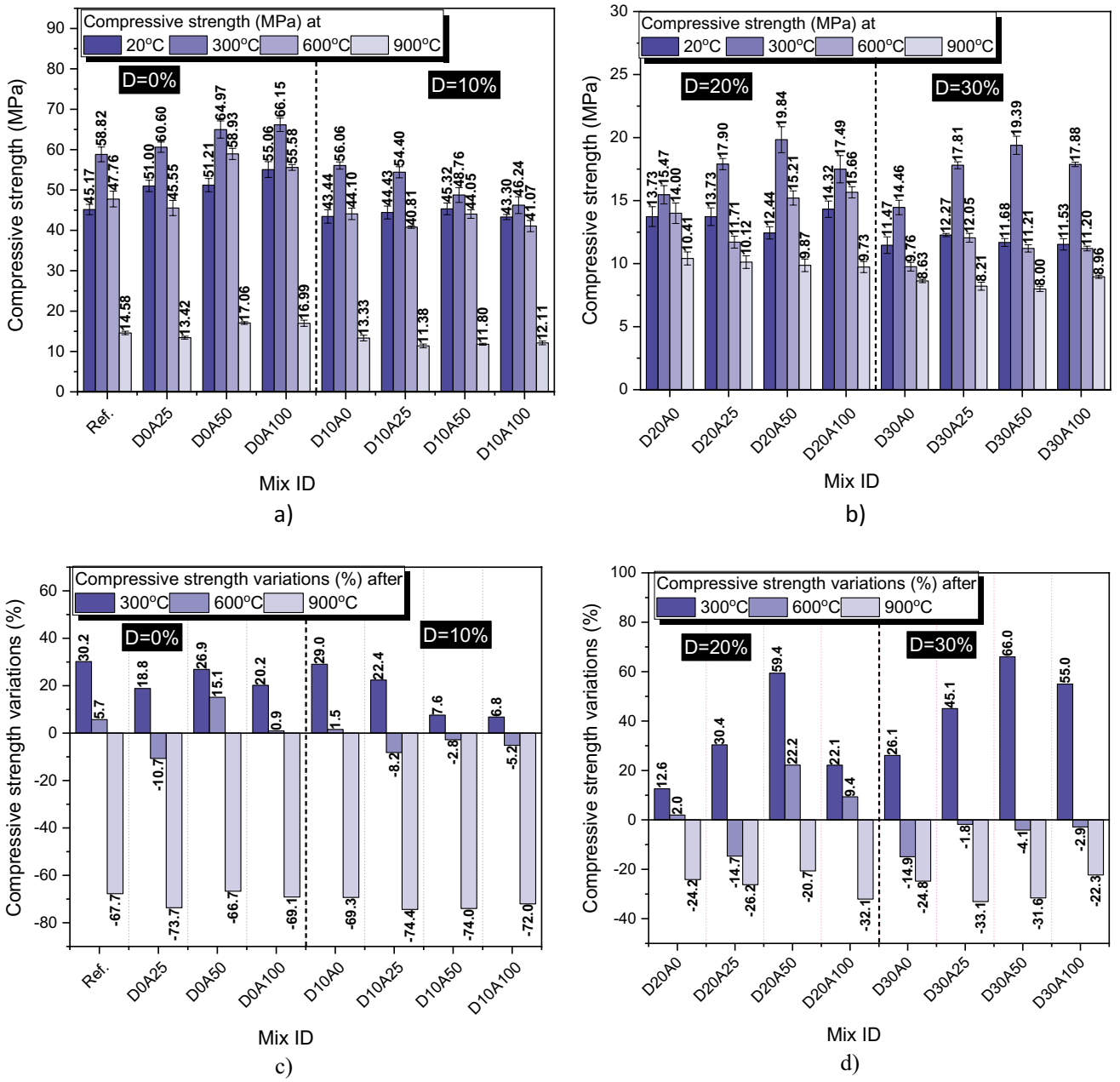

Fig. 13 Compressive strength and variations **a**, **c** at DP = 0% and 10% **b**, **d** at DP = 20% and 30% after elevated temperature

and increase their strength at these temperatures, accounts for this improvement [57]. In addition to internal autoclaving, vapor production and heating supports improved hydration, that improves chemical boundaries. Heat treatment of hardened AALC at 300 °C and 600 °C inevitably results in a hydrothermal reaction between unreacted GBFS grains and the remaining quantity of hydroxyl anions, driving geopolymerization processes, hydration and producing extra amounts of binding and/or thermally stable phases. The results obtained are completely consistent with other earlier investigations [64–67]. Contrary to compressive strength performance, the high-temperature resistance of AALC mixtures was greatly decreased in terms of flexural strength when GBFS was replaced with DP and more decrease in flexural strength was determined with increasing DP content after especially 900 °C. Addition of AS instead of SS generally showed negative effect on the flexural performance of AALC mixtures containing DP. At 0% DP content, the greatest high temperature resistance was determined for the mixtures without DP for all temperature ranges and the mixture D0A50 revealed the best performance with flexural strength enhancement of 31.9%, 28.8% and 0.3% at 300 °C, 600 °C,

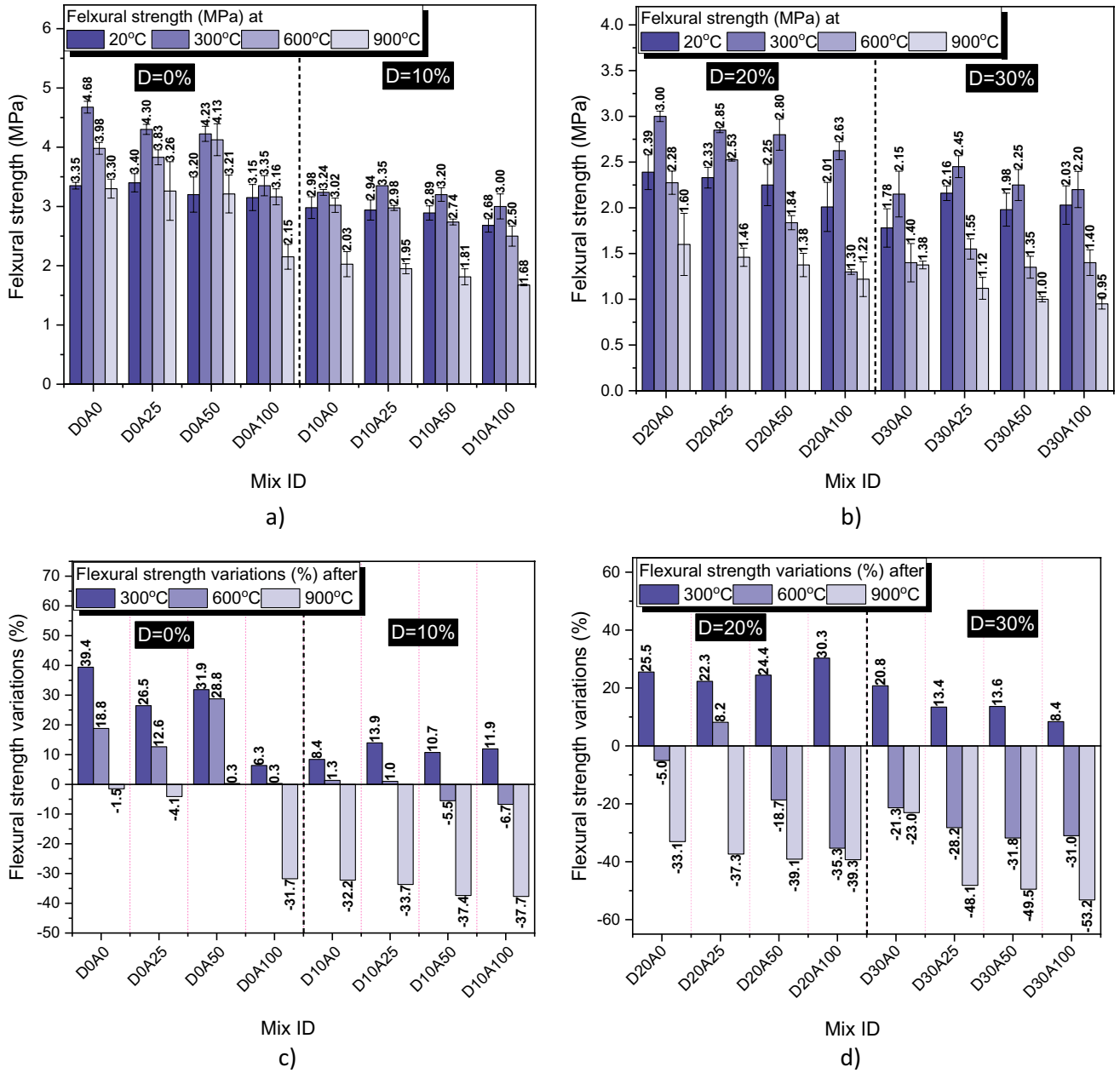

Fig. 14 Flexural strength and variations **a**, **c** at DP = 0% and 10% **b**, **d** at DP = 20% and 30% after elevated temperature

and 900 °C, respectively. However, the mixture with 100% AS had the worst resistance to high temperature at 900 °C at 0% DP content. At 10% DP content, the mixture D10A25 had the highest strength enhancement, with a strength increase of 13.9% and after 300 °C. As clearly seen that, strength reduction increased with increasing AS content at 900 °C and the worst performance was observed for the mixture D10A100 after 600 °C and 900 °C with strength reduction of 6.7% and 37.7%, respectively. At 20% DP content, the highest strength enhancement after 300 °C and the greatest strength reduction after 600 °C and 900 °C was observed for the same mixture containing 100% AS (D20A100). On the other hand, at 30% DP content, flexural strength enhancement with the inclusion of AS decreased with increasing content at 300 °C, flexural strength reduction with the inclusion of AS increased with increasing content after 600 °C and 900 °C. At this DP content, for all temperature ranges, the mixture D30A0 revealed the greatest performance at elevated temperatures. It can be concluded that increase in AS content affected flexural strength negatively with increasing DP content. This can be obviously explained by the fact that

the increasing porosity of the AALC mixtures with increase in DP and AS contents.

3.10.3 Mass loss

As denoted in Fig. 15a, b, the influence of andesite sand as a fine aggregate and DP as a precursor on the mean the mass loss of 28-day ambient cured AALC mixtures under high temperatures. The mass loss in all AALC mixtures increased as the temperature was raised. The results revealed that the mass loss of the AALC mixtures increased as DP and AS content increased. At 0% DP content, for the mixture containing 100% AS, notably after 600 °C, the largest mass loss following high temperature exposure was measured. The D0A100 resulted in mass decreases of up to 5.2% and 8.0% at 600 °C and 900 °C, respectively. At 10% DP content, similar results but more mass losses were obtained and the mixture containing 100% AS experienced the largest mass loss after being exposed to high temperatures, according to measurements. The D10A100 resulted in mass decreases of up to 6.5% and 8.8% at 600 °C and 900 °C, respectively. At 20% DP content, similar results but higher mass losses

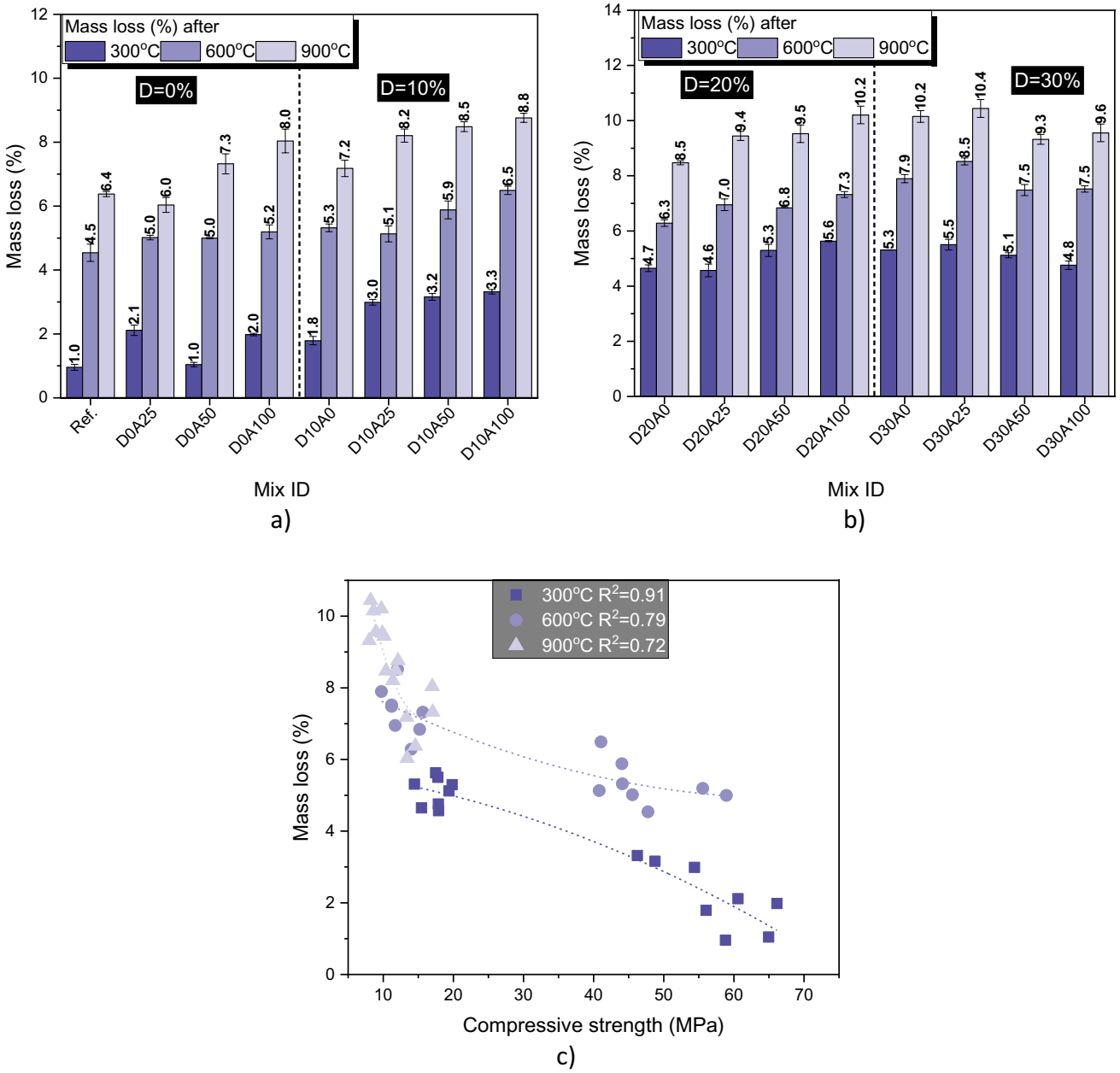

Fig. 15 Mass loss at **a** DP = 0% and 10% **b** DP = 20% and 30% **c** compressive strength vs. mass loss after elevated temperature

were achieved at 20% DP content, while the mixture containing 100% AS showed the highest mass loss under high temperatures. At 600 °C and 900 °C, the D20A100 caused mass losses of up to 7.3% and 10.2%, respectively. Contrary to other mixtures containing 0%, 10% and 20% DP, at 30% DP content, the mixture containing 25% AS demonstrated the maximum mass loss after being subjected to high temperatures. The D30A25 produced mass losses of up to 8.5% and 10.4%, respectively, at 600 °C and 900 °C. It was considered that weight losses at lower temperatures than calcite decarbonization correlate to water losses because no other component decomposes in GBFS–DP binders below 600 °C. Adsorbed water dissipates at around 150 °C, chemically bonded water disappears at about 300 °C, while OH groups can persist up to 700 °C [68, 69]. As can be observed in Fig. 15c, it was discovered that the relation among the compressive strength and mass loss of AALC mixtures had an R^2 values of 0.91, 0.79, and 0.72 at 300 °C, 600 °C, and 900 °C, respectively. Compressive strength and mass loss have a relation that appears to be inversely correlated with compressive strength.

3.10.4 Microstructural properties of mixtures exposed to high temperature

The microstructural properties of the reference mixture exposed to 900 °C are given in Fig. 16. After the high temperature, the number of micro cracks increased in the matrix. In addition, it was discovered that the micro crack's width expanded. Despite the application of 900 °C, some parts of the matrix observed the presence of N–A–S–H gels. It was determined in the microstructure studies that these gels were damaged at 900 °C but survived. The thermal conductivity coefficients of the mixtures could not reach the middle point of the 900 °C mortar, which is lower than the conventional concrete. In addition, the relatively high porosity slows down the spread of high heat.

There was noticeable high porosity in the matrix of the D10A50 mixture exposed to 900 °C (Fig. 17). It is thought that these voids originate from the 10% DP used in the mixture. When DP loses its water, it can turn into a porous structure. The diameter of these voids formed is usually less than 10 µm. Since the porosity increased with the effect of high temperature in these mixtures using DP, the diffusion of high heat slowed down even more. Therefore, it was determined that the N–A–S–H gels were relatively damaged in the

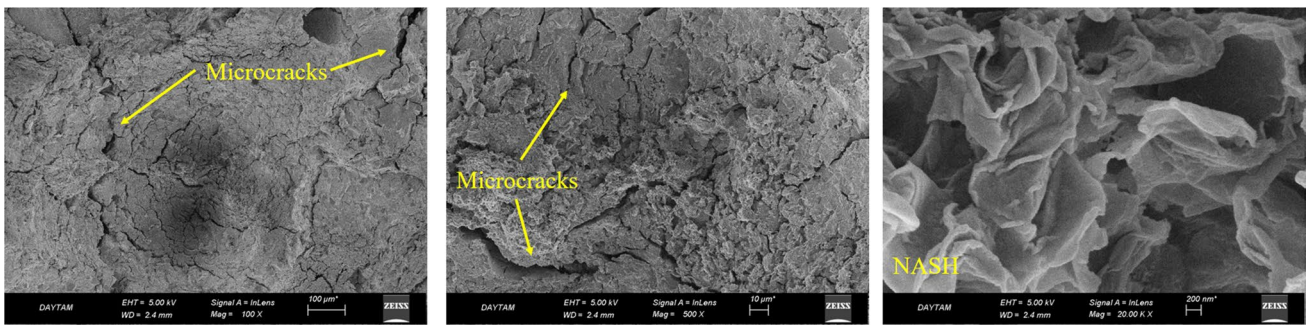

Fig. 16 Microstructure photos of the reference blend subjected to 900 °C

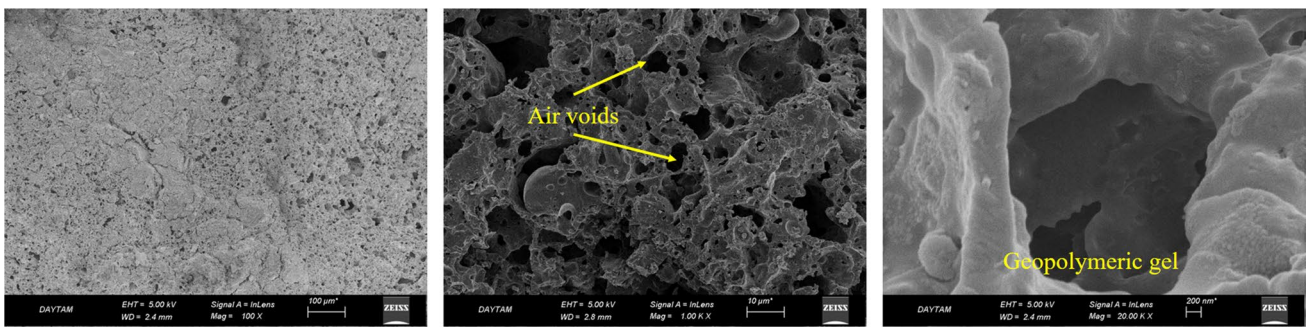

Fig. 17 Microstructure images of the D10A50 mixture exposed to 900 °C

matrix. However, DP was activated by the high-temperature effect and helped form a new geopolymeric gel.

Similar microstructure images were obtained in the D30A100 mixture using 30% DP (Fig. 18). As DP loses its constitutive water, it turns into a more porous form. In fact, pores larger than 10 µm have been detected on some surfaces. In addition, since the porosity of the D30A100 mixture using 30% DP increased, the thermal conductivity coefficient decreased. This reduced the temperature effect of 900 °C in the center of the mortar. Therefore, DP was activated at a lower temperature, formed geopolymeric gels, and maintained its presence in these gels up to 900 °C.

3.11 Freezing–thawing cycles

The characteristics of 28-day ambient cured AALC mixtures exposed to the F–T in the ranges of 40, 80, and 120 cycles were studied in relation to the effects of andesite sand as a fine aggregate and DP as a precursor in compliance to ASTM C666-97 [34], All mixes' samples, 40×40x160 mm in size, underwent freezing exposures at −20 ± 4 °C during 7 h in the air and 5 h of thawing in the water. This was done after 28 days of ambient-curing at 20 ± 3 °C. After performing F–T in the ranges of 40, 80, and 120 cycles, three samples of each mixture were examined for compressive, flexural strength, and mass loss.

3.11.1 Compressive strength

The term "freeze–thaw resistance" describes a material's capacity to tolerate extreme temperature changes, which can significantly affect their physical, mechanical, and durability properties. Due to the increased porosity and propensity of lightweight concrete to hold free water, F–T resistance can be a major source of durability problems. The degree of pore structure, the configuration of the pores, and the size of the pores all affect F–T resistance in AALC samples. More water absorption causes more ice to build up in the pores; when melting reduces pore volume and releases internal tension, the matrix walls experience compressive stress due to this expansion. Despite the fact that this test leads to an increase in pore widths and total porosity, the elastic/plastic stresses of the matrix result in the final volume change of the pores. Volume expansion and contraction-related loading and unloading can be modelled as fatigue loading [45, 49, 50, 70–72].The influence of andesite sand as a fine aggregate and DP as a precursor on the mean compressive strength of 28-day ambient cured AALC mixtures while exposed to F–T in the ranges of 0. 40, 80, and 120 cycles is illustrated in Fig. 19a, b. The variation in compressive strength under the influence of F–T cycles is demonstrated in Fig. 19c, d. All blends revealed strength gains after 40 F–T cycles, but after 120 F–T cycles, all mixtures indicated strength losses. This strength enhancement can be attributed to the continuing geopolymerization. At 0% DP content, the highest strength enhancement was measured for the mixture D0A25 with the strength increase of 21.6% and the second best resistance to 40 F–T cycles with strength increase of 20.1% was seen for the reference mixture that showed the worst resistance to freezing and thawing after 80 and 120 cycles with the highest strength loss. It seems that addition of AS instead of SS increased the freezing and thawing resistance of AALC mixtures and the mixture containing 50% AS had the least strength loss, which was found to be 19.3%. The best freeze–thaw resistance was observed for the mixtures containing 10% DP at all F–T ranges. The greatest strength enhancements after 40 and 80 F–T cycles were obtained for the mixture D10A0 and D10A25, respectively. On the other hand, the lowest strength reduction of 10.4% after 120 F–T cycles was experienced for the mixture containing 50% AS. It can be recorded that the optimum mixture for the freezing and thawing exposure was observed for the mixtures containing 10% DP as a substitute of GBFS. This results were supported by the previous study made by Degirmenc and Yılmaz [24]. The authors proved that mortars with 10% and 15% diatomite demonstrated greater resistance to damage from freezing and thawing. At 20%

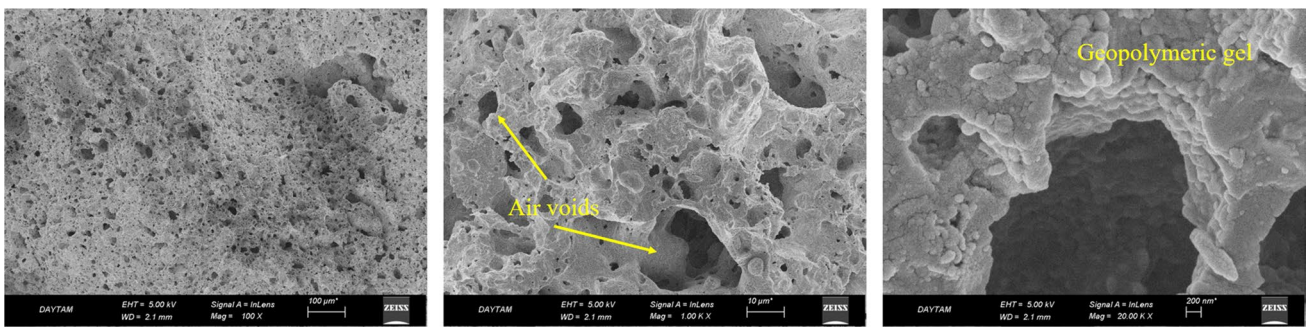

Fig. 18 Microstructure photos of the D30A100 blend subjected to 900 °C

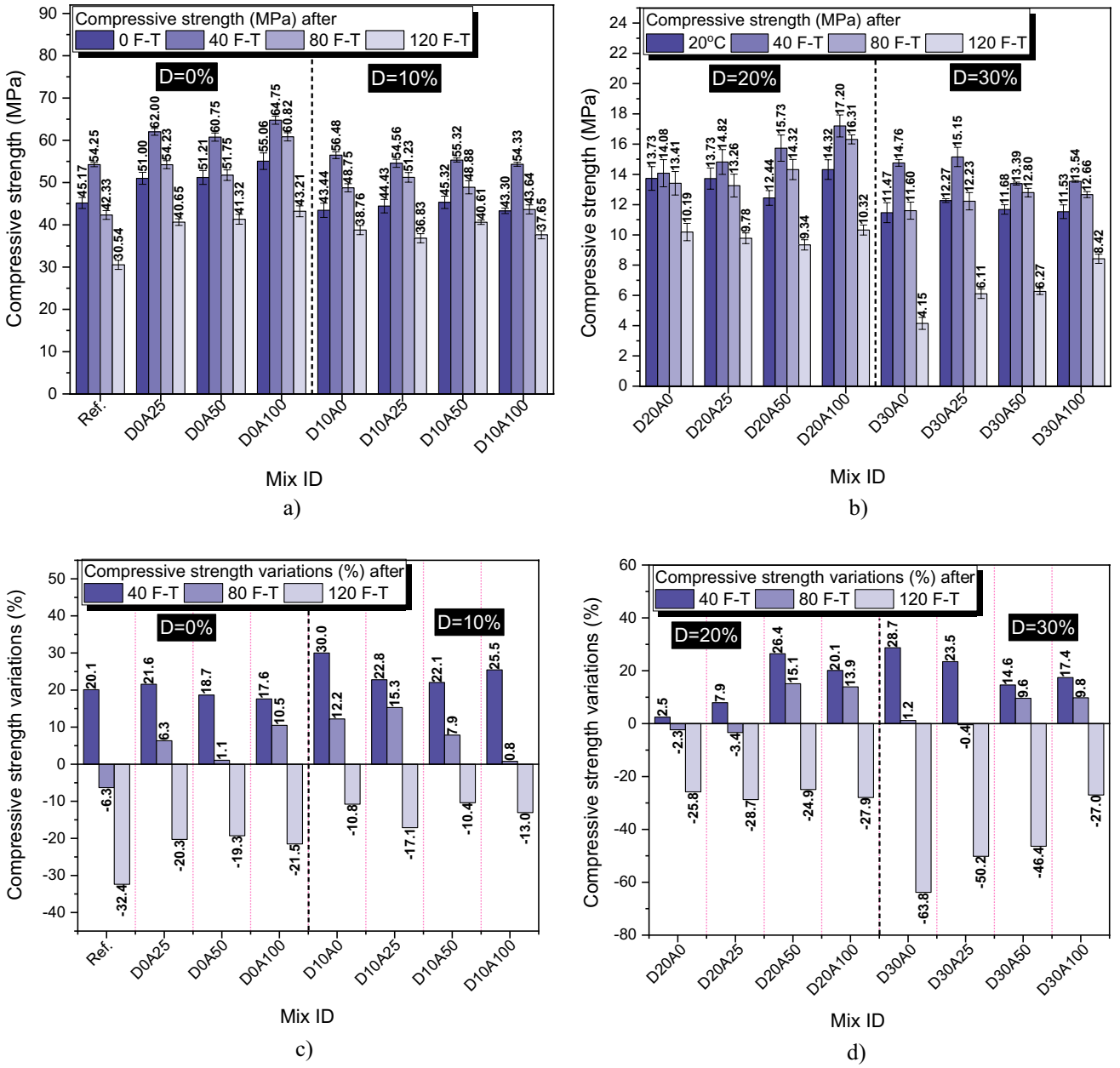

Fig. 19 Compressive strength and variations **a**, **c** at DP = 0% and 10% **b**, **d** at DP = 20% and 30% during freeze–thaw cycles

DP content, strength enhancement was also observed for all mixtures containing 20% DP after 40 F–T cycles and the highest strength enhancements were measured for the mixture D20A50 with the strength increments of 26.4% and 15.1% after 40 and 80 F–T cycles, respectively. The same mixture (i.e., D20A50) showed the least strength reduction when exposed to 120 F–T cycles. It is obvious that 0%, 10% and 20% DP incorporated mixtures containing 50% AS exhibited the best freeze–thaw resistance especially when exposed to 120 F–T cycles. After 40 F–T cycles, strength improvement was also seen for all mixes with 30% DP content and The mixture D30A0 showed the greatest strength improvement, with strength increases of 28.7% after 40 F–T cycles. Strength enhancement was reduced with increasing AS under 40 F–T cycles but increasing AS content improved the freezing and thawing resistance when the mixtures exposed more F–T cycles and the mixture D30A100 showed the least strength reduction when subjected to 80 and 120 F–T cycles. The protection of concrete to freeze and thaw can be achieved by air entrainment, as has been demonstrated. Reduced unit weight and greater porosity of the AS incorporated mixes relative to mixtures without AS were indicators of air entrainment [45, 49, 71, 72]. The results proved

that combined use of 50% AS instead of SS and 10% DP instead of GBFS performed the best freeze–thaw resistance among all mixtures.

3.11.2 Flexural strength

The influence of andesite sand as a fine aggregate and DP as a precursor on the mean flexural strength of 28-day ambient cured AALC mixtures after exposed to F–T in the ranges of 0, 40, 80 and 120 cycles is depicted in Fig. 20a, b. Figure 20c, d illustrates the strength variations after subjected to F–T cycles. All mixes showed increased strength after 40 F–T cycles as also observed for compressive strength; however, after 80 and 120 F–T cycles, all mixtures showed decreased strength. At 0% DP content, the greatest strength improvement was measured for the D0A25 blend with the strength increase of 25.0% as also seen in the compressive strength but the enhancement was reduced with increasing AS content after 40 F–T cycles. This increase in strength is caused by the continuing geopolymerization. While the mixtures exposed to 80 F–T, the lowest strength loss of 2.5% was seen for the mixture containing 50% AS. While the

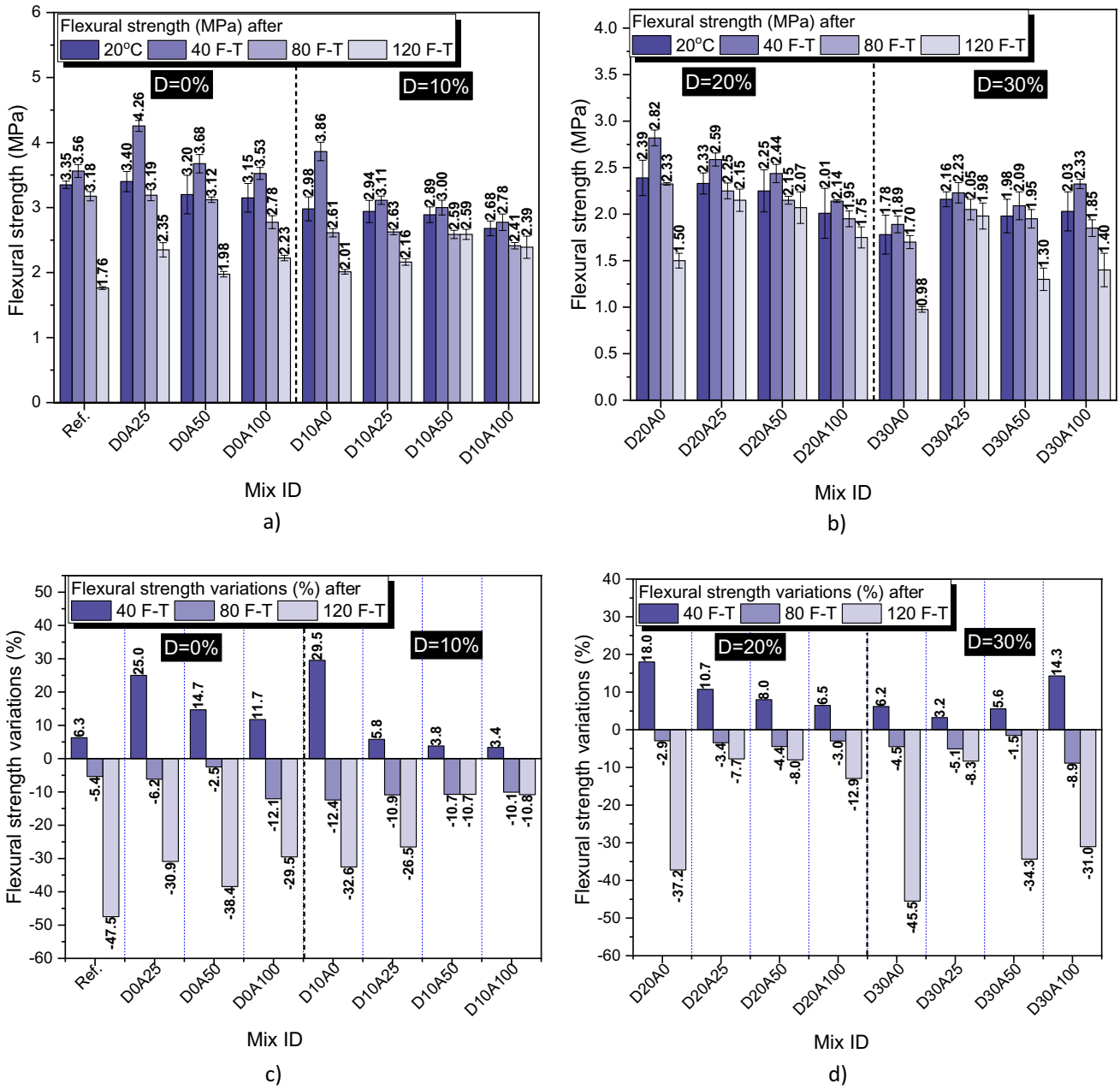

Fig. 20 Flexural strength and variations **a**, **c** at DP = 0% and 10% **b**, **d** at DP = 20% and 30% during freeze–thaw cycles

mixtures exposed to 120 F–T, the best resistance to F–T was seen for the mixture containing 100% AS meaning that using AS instead of SS. The mixture D10A0 showed the largest strength enhancement at 10% DP content, with a strength increase of 29.5%, which was also evident in the compressive strength after 40 F–T cycles. However, the enhancement decreased with increasing AS content after 40 F–T. This decrease in strength enhancement can be due to the decrease in geopolymerization with the addition of AS. On the other hand, replacing SS with 50% and 100% AS increased the F–T resistance notably after 80 and 120 F–T cycles with the strength loss of about 10%. Similar flexural strength behavior of AALC mixtures was also observed at 20% DP content. At 20% DP content, the mixture D20A0 had the strongest strength improvement, with a strength increase of 18.0%, which was also noticeable in the compressive strength after 40 F–T cycles. However, after 40 F–T, the enhancement became less significant while AS content increased. The blend D20A25 had the least strength loss of 7.7% and the best F–T performance among all AALC mixtures. At 30% DP content, the mixture D30A100 had the strongest strength enhancement contrary to the other mixtures with 10% and 20% DP content in which strength enhancement decreased with increasing AS content, with a strength increase of 14.3%. However, after 40 F–T, the enhancement became less significant while AS content decreased. With the least strength loss of 8.3%, the mixture D30A25 indicated the best F–T resistance at 30% DP content as seen in the mixtures with 20% DP content.

3.11.3 Mass loss

The mass variations of AALC mixtures, as shown in Fig. 21, was utilized to estimate the degree of AALC mixture deterioration brought on by F–T cycles. Under the influences of F–T in the ranges of 40, 80 and 120 cycles, all mixtures showed mass loss. More mass loss was observed with increasing F–T cycles. Addition of AS instead of SS also enhanced the mass loss of AALC samples due to the more porous structure of AS. Replacing GBFS with DP also enhanced the mass loss of AALC samples and the greatest mass loss was measured at 30% DP content after exposure of F–C cycles. This increase in mass loss could be the quick degradation of the internal structure of the samples. At 0% DP content, the greatest mass loss after F–T exposure was measured for the mixture containing 50% and 100% AS especially at 120 F–T cycles, as shown in Fig. 21a. The D0A100 mixture resulted in mass decreases of up to 2.1% and 12.2% at 80 and 120F–T, respectively. At 10% DP content, similar results but more mass losses were obtained and the greatest mass loss after 120 F–T exposure was measured for the mixture containing 100% AS. At 40 and 80 F–T cycles, mass loss of all mixtures containing 10% DP was very near to each other. At 20% DP content, similar results but higher mass losses were achieved at 20% DP content, while following 120 F–T cycles, the mixture containing 100% AS displayed the greatest mass loss, as shown in Fig. 21b. It seems that mass loss of the samples at this DP content showed no much difference between each other. Actually, it is evident that there were no significant differences in the mass loss of samples containing 20% and 30% DP at each F–T cycle. The results of compressive strength after F–T cycles observed in this investigation accord with the results of mass loss. Figure 21c depicts a direct link between compressive strength and mass loss of AALC samples, as in previous investigations [73, 74].

4 Conclusion

In this study, the impacts of waste andesite sand as a partial or full replacement for silica sand and diatomite powder as a partial replacement for GBFS on the mechanical, insulating, microstructural, and durability properties of alkali-activated lightweight composites (AALC) were explored. The main conclusions drawn according on the study's findings:

(a) For each DP content, the combination with 50% AS had the highest slump value, and the mixture without AS had the lowest slump value. The flowability of fresh AALC mixtures was reduced when GBFS was replaced with DP.
(b) It was determined that a mixture with 100% AS and no DP content had the highest compressive strength, which was around 60 MPa. The compressive strength of AALC mixes was significantly lowered using DP in place of GBFS.
(c) The dry unit weight of AALC mixtures decreased when GBFS was replaced with DP, and the mixtures with 30% DP had the lowest dry weight.
(d) The mixture D30A100 achieving the lowest thermal conductivity value makes it obvious that using DP in place of GBFS significantly enhanced porosity and decreased thermal conductivity.
(e) The mixture D30A50 had the maximum porosity and water absorption values when DP was used in place of GBFS.
(f) Apparently, the addition of DP greatly increased the specimens' shrinkage over the period of drying times. The AALC combinations without DP displayed the least amount of shrinkage of any mixture. When compared to the reference mixture, D0A100's dry shrinkage was 10.68% less at the end of the drying period, which was the lowest of the 2108 micro strains.

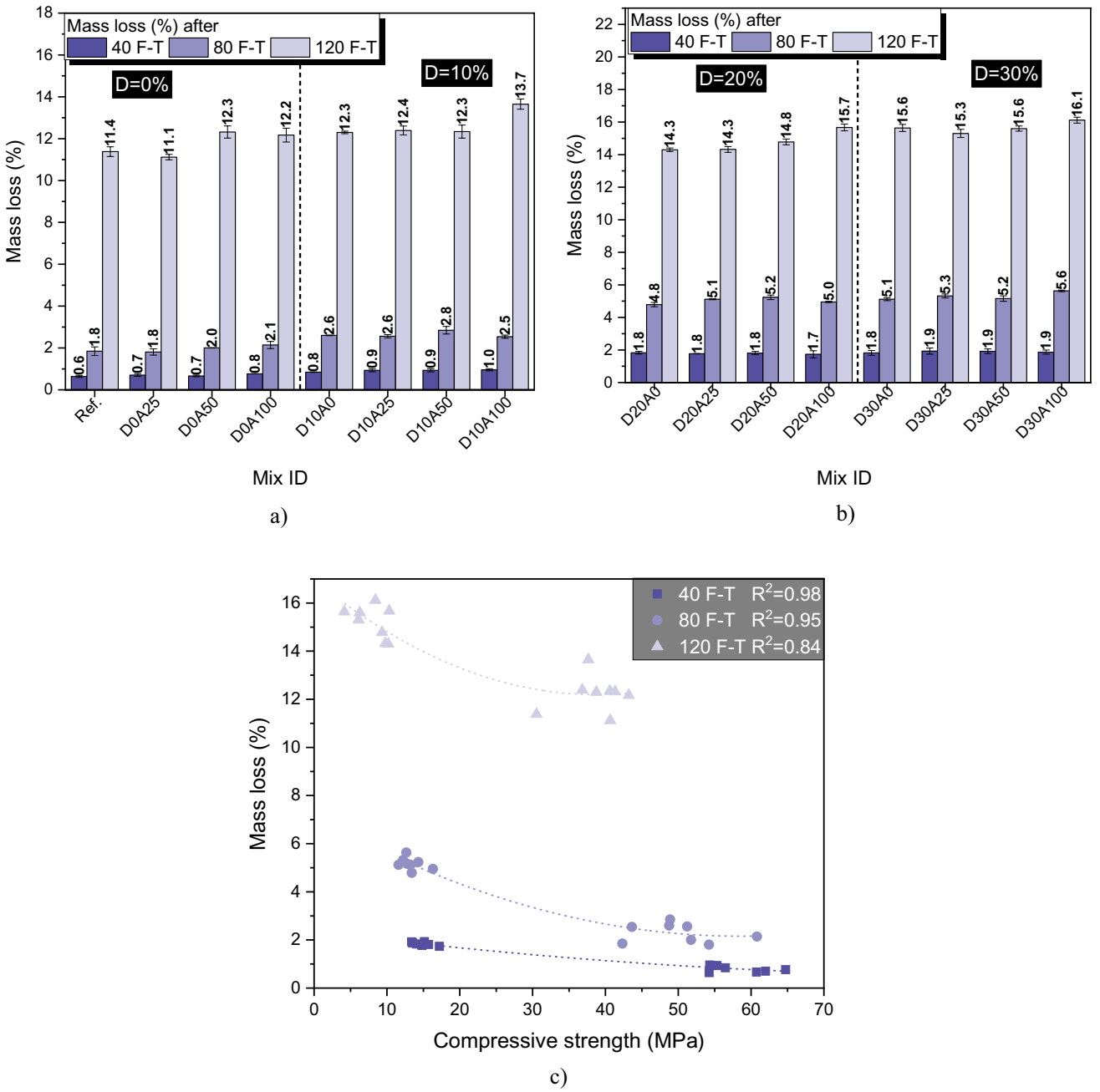

Fig. 21 Mass loss at **a** DP = 0% and 10%, **b** DP = 20% and 30%, **c** compressive strength vs. mass loss during freeze–thaw cycles

(g) At the end of the 28-day ambient curing, the AALC mixture without DP and containing 100% AS (D0A100) displayed the lowest sorptivity value of 11.76 mm/s$^{0.5}$, a 14.65% decline from the reference mixture.

(h) Among the AALC mixes, the mixture D20A50 (containing 20% DP and 50% AS) demonstrated a compressive strength gain notably by 59.4% and 22.2% at 300 °C and 600 °C, respectively. It also displayed the lowest strength loss of 20.7% at 900 °C.

(i) It should be noted that the combinations containing 10% DP as a replacement for GBFS were found to be the best mixture for exposure to freezing and thawing. The greatest strength enhancements after 40 and 80 F–T cycles were determined for the mixture D10A0 and D10A25, respectively. The optimum mixture for the freezing and thawing exposure was observed for the mixtures containing 10% DP as a substitute of GBFS.

5 Limitations of the study and recommendation for further studies

Although a comprehensive experimental program was carried out in the present research, this study has some limited points. One of them is the number of freeze–thaw cycles designated as 40, 80, and 120 cycles in the scope of the current study. The mixtures manufactured herein may have been exposed to further freezing–thawing processes. In addition, determining the durability of the mixtures in terms of only freezing–thawing resistance can be considered the second limited point of the study. The durability performance of the mixtures against sulfate and chloride attacks may also have been investigated. Besides, determining the mechanical properties of the mixtures by only compressive and flexural strengths can be regarded as another limited point. The modulus of elasticity values and Poisson's ratios of the mixtures may also have been determined. In this context, it may be recommended for the researchers studying this topic that aforementioned properties and experimental program may be considered in their investigations.

Funding This research received no external funding.

Data availability The data that support the findings of this study are available from the corresponding author upon reasonable request.

Declarations

Conflict of interest The author declares that he has no conflict of interest.

Ethical approval This article does not contain any studies with human participants or animals performed by any of the authors.

References

1. Huseien GF, Hamzah HK, Sam ARM, Khalid NHA, Shah KW, Deogrescu DP, et al. Alkali-activated mortars blended with glass bottle waste nano powder: environmental benefit and sustainability. J Clean Prod. 2020;243:118636.
2. Zhao Z, Grellier A, El Karim BM, Michel F, Bulteel D, Courard L. Substitution of limestone filler by waste brick powder in self-compacting mortars: properties and durability. J Build Eng. 2021;43:102898.
3. Zhang H-Y, Liu J-C, Wu B. Mechanical properties and reaction mechanism of one-part geopolymer mortars. Constr Build Mater. 2021;273:121973.
4. Yehualaw MD, Hwang CL, Vo DH, Koyenga A. Effect of alkali activator concentration on waste brick powder-based ecofriendly mortar cured at ambient temperature. J Mater Cycles Waste Manage. 2021;23(2):727–40.
5. Albidah AS. Effect of partial replacement of geopolymer binder materials on the fresh and mechanical properties: a review. Ceram Int. 2021;47(11):14923–43.
6. Hottle T, Hawkins TR, Chiquelin C, Lange B, Young B, Sun P, et al. Environmental life-cycle assessment of concrete produced in the United States. J Clean Prod. 2022;363: 131834.
7. Alsaif A, Albidah A, Abadel A, Abbas H, Al-Salloum Y. Development of metakaolin-based geopolymer rubberized concrete: fresh and hardened properties. Arch Civ Mech Eng. 2022. https://doi.org/10.1007/s43452-022-00464-y.
8. Reddy KC, Subramaniam KVL. Investigation on the roles of solution-based alkali and silica in activated low-calcium fly ash and slag blends. Cem Concr Comp. 2021. https://doi.org/10.1016/j.cemconcomp.2021.104175.
9. Karatas M, Dener M, Mohabbi M, Benli A. A study on the compressive strength and microstructure characteristic of alkali-activated metakaolin cement. Materia-Brazil. 2019. https://doi.org/10.1590/s1517-707620190004.0832.
10. Turkoglu M, Bayraktar OY, Benli A, Kaplan G. Effect of cement clinker type, curing regime and activator dosage on the performance of one-part alkali-activated hybrid slag/clinker composites. J Build Eng. 2023;68: 106164.
11. Bayrak B, Benli A, Alcan HG, Çelebi O, Kaplan G, Aydın AC. Recycling of waste marble powder and waste colemanite in ternary-blended green geopolymer composites: Mechanical, durability and microstructural properties. J Build Eng. 2023;73: 106661.
12. Koksal F, Bayraktar OY, Bodur B, Benli A, Kaplan G. Insulating and fire-resistant performance of slag and brick powder based one-part alkali-activated lightweight mortars. Struct Concr. 2022;24(3):3128–46.
13. Provis JL. Alkali-activated materials. Cem Concr Res. 2018;114:40–8.
14. Casanova S, Silva RV, de Brito J, Pereira MFC. Mortars with alkali-activated municipal solid waste incinerator bottom ash and fine recycled aggregates. J Clean Prod. 2021;289: 125707.
15. Long WJ, Peng JK, Gu YC, Li JL, Dong BQ, Xing F, et al. Recycled use of municipal solid waste incinerator fly ash and ferronickel slag for eco-friendly mortar through geopolymer technology. J Clean Prod. 2021;307: 127281.
16. Gonzalez-Garcia DM, Tellez-Jurado L, Jimenez-Alvarez FJ, Zarazua-Villalobos L, Balmori-Ramirez H. Evolution of a natural pozzolan-based geopolymer alkalized in the presence of sodium or potassium silicate/hydroxide solution. Constr Build Mater. 2022;321: 126305.
17. Miller SA, John VM, Pacca SA, Horvath A. Carbon dioxide reduction potential in the global cement industry by 2050. Cem Concr Res. 2018;114:115–24.
18. Zhang ZH. Composites Part B-special issue: alkali activated materials and composites. Compos Part B Eng. 2023;257: 110690.
19. Zhang XY, Fan M, Zhou Y, Ji D, Li J, Yu R. Development of a sustainable alkali activated ultra-high performance concrete (A-UHPC) incorporating recycled concrete fines. J Build Eng. 2023;67: 105986.
20. Zhang P, Han X, Hu SW, Wang J, Wang TY. High-temperature behavior of polyvinyl alcohol fiber-reinforced metakaolin/fly ash-based geopolymer mortar. Compos Part B Eng. 2022;244: 110171.
21. Li L, Wei YJ, Li ZL, Farooqi MU. Rheological and viscoelastic characterizations of fly ash/slag/silica fume-based geopolymer. J Clean Prod. 2022;354: 131629.
22. Gultekin A, Ramyar K. Investigation of high-temperature resistance of natural pozzolan-based geopolymers produced with oven and microwave curing. Constr Build Mater. 2023;365: 130059.
23. Thammarong S, Lertcumfu N, Jaita P, Manotham S, Tunkasiri T, Pimpha N, et al. The effects of replacement metakaolin with diatomite in geopolymer materials. Key Eng Mater. 2019;798:267–72.
24. Kipsanai JJ, Wambua PM, Namango SS, Amziane S. A review on the incorporation of diatomaceous earth as a geopolymer-based concrete building resource. Mater Des. 2022;15(20):7130.

25. Lee M-G, Huang Y, Shih Y-F, Wang W-C, Wang Y-C, Wang Y-X, et al. Mechanical and thermal insulation performance of waste diatomite cement mortar. J Market Res. 2023;25:4739–48.
26. Özsoy A, Örklemez E, İlkentapar S. Effect of addition diatomite powder on mechanical strength, elevated temperature resistance and microstructural properties of industrial waste fly ash-based geopolymer. J Mater Cycles Waste Manag. 2023;25(4):2338–49.
27. Davraz M, Ceylan H, Topcu IB, Uygunoglu T. Pozzolanic effect of andesite waste powder on mechanical properties of high strength concrete. Constr Build Mater. 2018;165:494–503.
28. Celikten S. Mechanical and microstructural properties of waste andesite dust-based geopolymer mortars. Adv Powder Technol. 2021;32(1):1–9.
29. Özkan Ş, Ceylan H. The effects on mechanical properties of sustainable use of waste andesite dust as a partial substitution of cement in cementitious composites. J Build Eng. 2022;58: 104959.
30. ASTM C1437-15 Standard test method for flow of hydraulic cement mortar. ASTM International: West Conshohocken, PA. 2015.
31. ASTM C642-13 Standard test method for density, absorption, and voids in hardened concrete. ASTM International; West Conshohocken, PA. 2013.
32. ASTM C348-19 Standard test method for flexural strength of hydraulic-cement mortars. ASTM International, West Conshohocken, PA. 2019.
33. ASTM C349-18 Standard test method for compressive strength of hydraulic-cement mortars (Using Portions of Prisms Broken in Flexure). ASTM International, West Conshohocken, PA. 2018.
34. ASTM C 666-97, Standard test method for resistance of concrete to rapid freezing and thawing. ASTM International; West Conshohocken, PA. 2015.
35. ASTM C1585-20 Standard test method for measurement of rate of absorption of water by hydraulic-cement concretes, West Conshohocken, PA: ASTM International. 2020.
36. ASTM C596-18 Standard test method for drying shrinkage of mortar containing hydraulic cement, West Conshohocken, ASTM International: PA. 2018.
37. ASTM D7984-16 Standard test method for measurement of thermal effusivity of fabrics using a modified transient plane source (MTPS) Instrumen, ASTM International. 2016.
38. Zahra A, Jamshid E, Jamil K, Robab H. Properties of sustainable cement mortars containing a high volume of raw diatomite. Sust Sust Mater Technol. 2018;16:47–53.
39. Sharma N, Sharma P, kr Verma S, editors. Influence of Diatomite on the properties of mortar and concrete: a review. IOP Conference Series: materials science and engineering; 2021: IOP Publishing.
40. Hamidi M, Kacimi L, Cyr M, Clastres P. Evaluation and improvement of pozzolanic activity of andesite for its use in eco-efficient cement. Constr Build Mater. 2013;47:1268–77.
41. Degirmenci N, Yilmaz A. Use of diatomite as partial replacement for Portland cement in cement mortars. Constr Build Mater. 2009;23(1):284–8.
42. Phoo-ngernkham T, Chindaprasirt P, Sata V, Sinsiri T. High calcium fly ash geopolymer containing diatomite as additive. Indian J Eng Mater S. 2013;20(4):310–8.
43. Kearsley EP, Wainwright PJ. The effect of porosity on the strength of foamed concrete. Cem Concr Res. 2002;32(2):233–9.
44. Bayrak B, Öz A, Benli A, Kavaz E, Kaplan G, Aydın AC. Physico-mechanical and shielding properties of alkali-activated slag composites incorporating cement clinker aggregate: effect of high temperature and particle size. J Build Eng. 2023;67: 105982.
45. Gencel O, Benli A, Bayraktar OY, Kaplan G, Sutcu M, Elabade WAT. Effect of waste marble powder and rice husk ash on the microstructural, physico-mechanical and transport properties of foam concretes exposed to high temperatures and freeze-thaw cycles. Constr Build Mater. 2021;291: 123374.
46. Demirboga R. Influence of mineral admixtures on thermal conductivity and compressive strength of mortar. Energy Build. 2003;35(2):189–92.
47. Demirboga R. Thermal conductivity and compressive strength of concrete incorporation with mineral admixtures. Build Environ. 2007;42(7):2467–71.
48. Corinaldesi V, Mazzoli A, Moriconi G. Mechanical behaviour and thermal conductivity of mortars containing waste rubber particles. Mater Des. 2011;32(3):1646–50.
49. Bayraktar OY, Soylemez H, Kaplan G, Benli A, Gencel O, Turkoglu M. Effect of cement dosage and waste tire rubber on the mechanical, transport and abrasion characteristics of foam concretes subjected to H2SO4 and freeze-thaw. Constr Build Mater. 2021;302: 124229.
50. Bayraktar OY, Kaplan G, Gencel O, Benli A, Sutcu M. Physico-mechanical, durability and thermal properties of basalt fiber reinforced foamed concrete containing waste marble powder and slag. Constr Build Mater. 2021;288: 123128.
51. You GL, Bi JQ, Chen YF, Yin CL, Wang CA. Effect of diatomite additive on the mechanical and dielectric properties of porous SiO2-Si3N4 composite ceramics. J Wuhan Univ Technol. 2016;31(3):528–32.
52. Gencel O, Nodehi M, Bayraktar OY, Kaplan G, Benli A, Gholampour A, et al. Basalt fiber-reinforced foam concrete containing silica fume: An experimental study. Constr Build Mater. 2022;326: 126861.
53. Gencel O, Bayraktar OY, Kaplan G, Arslan O, Nodehi M, Benli A, et al. Lightweight foam concrete containing expanded perlite and glass sand: Physico-mechanical, durability, and insulation properties. Constr Build Mater. 2022;320: 126187.
54. Xue LL, Zhang ZH, Liu HF, Jiang YH, Wang H. Drying shrinkage behavior of hybrid alkali activated cement (HAAC) mortars. Constr Build Mater. 2022;316: 126068.
55. Neto AAM, Cincotto MA, Repette W. Drying and autogenous shrinkage of pastes and mortars with activated slag cement. Cem Concr Res. 2008;38(4):565–74.
56. Collins F, Sanjayan JG. Effect of pore size distribution on drying shrinkage of alkali-activated slag concrete. Cem Concr Res. 2000;30(9):1401–6.
57. Song QF, Guo MZ, Ling TC. A review of elevated-temperature properties of alternative binders: Supplementary cementitious materials and alkali-activated materials. Constr Build Mater. 2022;341: 127894.
58. Benli A, Karatas M, Toprak HA. Mechanical characteristics of self-compacting mortars with raw and expanded vermiculite as partial cement replacement at elevated temperatures. Constr Build Mater. 2020;239: 117895.
59. Karatas M, Benli A, Toprak HA. Effect of incorporation of raw vermiculite as partial sand replacement on the properties of self-compacting mortars at elevated temperature. Constr Build Mater. 2019;221:163–76.
60. Koksal F, Nazli T, Benli A, Gencel O, Kaplan G. The effects of cement type and expanded vermiculite powder on the thermo-mechanical characteristics and durability of lightweight mortars at high temperature and RSM modelling. Case Stud Constr Mater. 2021;15:e00709.
61. Koksal F, Gencel O, Brostow W, Lobland HEH. Effect of high temperature on mechanical and physical properties of lightweight cement based refractory including expanded vermiculite. Mater Res Innovations. 2013;16(1):7–13.
62. Koksal F, Gencel O, Kaya M. Combined effect of silica fume and expanded vermiculite on properties of lightweight mortars at ambient and elevated temperatures. Constr Build Mater. 2015;88:175–87.

63. Qin Y, Leng GH, Yu X, Cao H, Qiao G, Dai YF, et al. Sodium sulfate-diatomite composite materials for high temperature thermal energy storage. Powder Technol. 2015;282:37–42.
64. Ramadan M, Amin MS, Waly SA, Mohsen A. Effect of high gamma radiation dosage and elevated temperature on the mechanical performance of sustainable alkali-activated composite as a cleaner product. Cem Concr Comp. 2021;121: 104087.
65. Rashad AM, Sadek DM, Hassan HA. An investigation on blast-furnace stag as fine aggregate in alkali-activated slag mortars subjected to elevated temperatures. J Clean Prod. 2016;112:1086–96.
66. Bakharev T, Sanjayan JG, Cheng YB. Effect of elevated temperature curing on properties of alkali-activated slag concrete. Cem Concr Res. 1999;29(10):1619–25.
67. Aydin S, Baradan B. High temperature resistance of alkali-activated slag- and portland cement-based reactive powder concrete. Aci Mater J. 2012;109(4):463–70.
68. Perez-Cortes P, Cabrera-Luna K, Escalante-Garcia JI. Alkali-activated limestone/metakaolin cements exposed to high temperatures: Structural changes. Cem Concr Comp. 2021;122:104147.
69. Duxson P, Lukey GC, van Deventer JSJ. Physical evolution of Na-geopolymer derived from metakaolin up to 1000 degrees C. J Mater Sci. 2007;42(9):3044–54.
70. Abdollahnejad Z, Mastali M, Woof B, Illikainen M. High strength fiber reinforced one-part alkali activated slag/fly ash binders with ceramic aggregates: Microscopic analysis, mechanical properties, drying shrinkage, and freeze-thaw resistance. Constr Build Mater, 2020; 241.
71. Bayraktar OY, Eshtewi SST, Benli A, Kaplan G, Toklu K, Gunek F. The impact of RCA and fly ash on the mechanical and durability properties of polypropylene fibre-reinforced concrete exposed to freeze-thaw cycles and $MgSO_4$ with ANN modeling. Constr Build Mater. 2021;313: 125508.
72. Bayraktar OY, Kaplan G, Benli A. The effect of recycled fine aggregates treated as washed, less washed and unwashed on the mechanical and durability characteristics of concrete under $MgSO_4$ and freeze-thaw cycles. J Build Eng. 2022;48: 103924.
73. Gencel O, Bayraktar OY, Kaplan G, Benli A, Martinez-Barrera G, Brostow W, et al. Characteristics of hemp fibre reinforced foam concretes with fly ash and Taguchi optimization. Constr Build Mater. 2021;294: 123607.
74. Kaplan G, Coskan U, Benli A, Bayraktar OY, Kucukbaltaci AB. The impact of natural and calcined zeolites on the mechanical and durability characteristics of glass fiber reinforced cement composites. Constr Build Mater. 2021;311: 125336.